Erosion of Archean continents: The Sm-Nd and Lu-Hf isotopic record of Barberton sedimentary rocks

Marion Garçon, R.W. Carlson, S.B. Shirey, N.T. Arndt, M.F. Horan, T.D. Mock

Erosion of Archean continents: The Sm-Nd and Lu-Hf isotopic record of Barberton sedimentary rocks

M. Garçon[1]*, R.W. Carlson[1], S.B. Shirey[1], N.T. Arndt[2], M.F. Horan[1], T. D. Mock[1]

[1] Carnegie Institution for Science, Department of Terrestrial Magnetism, 5241 Broad Branch Road, NW, Washington DC 20015-1305, United States

[2] ISTerre, UMR 5275, CNRS, Université Grenoble-Alpes, BP 53, FR-38041 Grenoble CEDEX 09, France

* *Corresponding author*
Now at: ETH Zürich, Department of Earth Sciences, Institute of Geochemistry and Petrology, Clausiusstrasse 25, 8092 Zürich, Switzerland
E-mail: marion.garcon@erdw.ethz.ch

Abstract

Knowing the composition, nature and amount of crust at the surface of the early Earth is crucial to understanding the early geodynamics of our planet. Yet our knowledge of the Hadean-Archean crust is far from complete, limited by the poor preservation of Archean terranes, and the fact that less attention has been paid to the sedimentary record that tracks erosion of these ancient remnants. To address this problem and get a more comprehensive view of what an Archean continent may have looked like, we investigated the trace element and Sm-Nd, Lu-Hf isotopic records of Archean metasedimentary rocks from South Africa. We focused our study on sandstone and mudstone from drill core in the Fig Tree Group (3.23-3.26 Ga) of the Barberton granite-greenstone belt, but also analyzed the 3.4 Ga Buck Reef cherts and still older (3.5–3.6 Ga) meta-igneous rocks from the Ancient Gneiss Complex, Swaziland.

Based on principal component analysis of major and trace element data, the Fig Tree metasedimentary rocks can be classified into three groups: crustal detritus-rich sediments, Si-rich sediments and Ca-, Fe-rich sediments. The detritus-rich sediments have preserved the Sm-Nd and Lu-Hf isotopic signatures of their continental sources, and hence can be used to constrain the composition of crust eroded in the Barberton area in the Paleoarchean period. Based on Sm/Nd ratios, we estimate that this crust was more mafic than today, with an

average SiO_2 content of 60.5 ± 2 wt.%. This composition is further supported by isotopic mixing calculations suggesting that the sedimentary source area contained equal proportions of mafic-ultramafic and felsic rocks. This implies that the Archean crust exposed to weathering was more mafic than today but does not exclude a more felsic composition at depth. Neodymium and Hf crustal residence ages show that the eroded crust was, on average, ~300-400 Ma older than the deposition age of the sediments, which highlights the importance of intracrustal reworking of older crust at ~3.2 Ga in the Barberton area.

The Si-rich sediments have slightly positive $\varepsilon_{Nd\ (t=3.23Ga)}$ but extremely radiogenic $\varepsilon_{Hf\ (t=3.23Ga)}$, up to +11. Based on analyses of 3.4 Ga Buck Reef cherts, we suggest that the radiogenic Hf isotopic signature of the Si-rich sediments can be accounted for by the old chert clasts or detrital silicified rock fragments present in the rocks. The latter have extremely high Lu/Hf ratios such that their ε_{Hf} values would increase dramatically, by about +100 epsilon units every 100 Ma. In the Ca-, Fe-rich sediments, one sample contains carbonate that preserves the typical rare-earth element features of seawater precipitates. The initial Nd isotopic composition of this sample ($\varepsilon_{Nd\ (t=3.23Ga)}$ = +1.7) is within the range of previous estimates for Archean anoxic seawater.

Keywords: Neodymium, Hafnium, Continental crust, Chert, Fig Tree group

1. Introduction

Archean sedimentary rocks and their metamorphic equivalents are made up of rock fragments and minerals derived from the erosion of ancient continents and/or precipitates from fluids such as seawater. In contrast to igneous rocks, their composition has the potential to reflect a greater spectrum of materials that were exposed at the surface of the early Earth, including lithologies that are no longer present at the surface. Trace and major element contents of Archean sedimentary rocks have previously provided important information on the composition of the early crust and oceans as well as the oxidation state of the atmosphere-ocean system (Taylor and McLennan, 1985; Condie, 1993; Kamber and Webb, 2001; Bolhar et al., 2005; Hofmann, 2005; Alexander et al., 2009; Bau and Alexander, 2009; Kamber, 2010; Thurston et al., 2012; Kamber et al., 2014; Gaschnig et al., 2014; Liu et al., 2015; Tang et al., 2016; Gaschnig et al., 2016). In general, these studies suggest that the upper Archean crust was more mafic, and that the oceans were anoxic and dominated by higher hydrothermal

inputs than today. The Sm-Nd isotopic systematics of Archean sedimentary rocks have brought complementary constraints on the nature and average crustal residence age of the upper Archean crust (e.g. Jacobsen and Dymek, 1988; Frost, 1993; Jahn and Condie, 1995; Yamashita and Creaser, 1999; Yamashita et al., 2000). Most of the Sm-Nd data converge towards the conclusion that ancient sediments received important contributions from older continental crustal material, implying that enough felsic crust had formed in the early Archean to be registered in their sedimentary provenance. This interpretation receives some support from *in situ* Lu-Hf isotopic analyses of detrital and magmatic Archean zircons (Belousova et al., 2010; Griffin et al., 2014) even though the latter have more variable compositions and may record a higher contribution of juvenile material in the early Archean.

In this paper, we report trace element concentrations and coupled whole-rock Lu-Hf and Sm-Nd isotopic analyses of Archean metasedimentary rocks to see whether the two isotopic systems when used in combination, can provide new insights on the crustal composition and evolution of the Eastern Kaapvaal craton and potentially the composition of Paleoarchean seawater. Except for the few measurements reported for example by Vervoort et al. (1999), Hoffman et al. (2010) and Viehmann et al. (2014), whole-rock Lu-Hf isotopic compositions of ancient metasedimentary rocks have generally not been measured. Most studies have concentrated instead on *in situ* Lu-Hf isotopic analyses of detrital Archean zircons. This approach, however, may capture the composition of only the most felsic portions of the Archean crust, because zircons are common in felsic magmas, but very rare in mafic ones. Here, we chose to investigate whole-rock Lu-Hf isotopic systematics rather than *in situ* analyses of zircons to get a more comprehensive view of the composition of the eroded crust and oceans in the Barberton area and to facilitate the comparison of Sm-Nd and Lu-Hf isotopic data.

Use of sedimentary rocks as natural samples of the average composition of surrounding crust requires a careful evaluation of the effect of sedimentary processes. While weathering and post-depositional processes are generally well discussed in most studies dealing with Archean rocks, the effects of other sedimentary processes such as different erodibility of mafic and felsic rocks, or mineral sorting during sediment transport, are not systematically evaluated by geochemists. Yet, these processes have been shown to bias the composition of modern sediments and significantly affect interpretations of sediment provenance (e.g. Patchett et al., 1984; Garzanti et al., 2010; Garzanti et al., 2011; Dhuime et al., 2011; Garçon et al., 2013; Garçon et al., 2014; Sauzéat et al., 2015). Here, we evaluate and correct for sedimentary

effects in order to extract valuable information from the Archean sedimentary record.

This study focuses on Paleoarchean sedimentary samples – mainly sandstones and mudstones – from core obtained by the International Continental Scientific Drilling Program (ICDP) in the Fig Tree Group of the Barberton granite-greenstone belt, in the eastern part of the Kaapvaal Craton in South Africa. The Barberton granite-greenstone belt is an emblematic Paleoarchean terrane. Its outcrops of plutonic and volcanic rocks, in particular the komatiite sequences, have been widely studied for their chemical and isotopic compositions (Condie and Hunter, 1976; Clemens et al., 2006; Grosch et al., 2011; Stiegler et al., 2012; Furnes et al., 2012; Robin-Popieul et al., 2012; Furnes et al., 2013; Kröner et al., 2013), including whole-rock Sm-Nd and Lu-Hf isotopic analyses (Lahaye et al., 1995; Chavagnac, 2004; Clemens et al., 2006; Van Kranendonk et al., 2009; Puchtel et al., 2013; Kröner et al., 2013; Blichert-Toft et al., 2015). Investigations of Barberton metasedimentary rocks, however, are scarcer although they are among the best-preserved Paleoarchean sedimentary sequences that can be found on Earth. In particular, Fig Tree metasedimentary rocks have been studied for trace and major element concentrations (Condie et al., 1970; Toulkeridis et al., 1999; Hofmann, 2005) and *in situ* Lu-Hf isotopic analyses on zircons separated from one coarse-grained greywacke (Zeh et al., 2013). Only a small number of whole-rock Rb-Sr, Sm-Nd and Pb-Pb isotopic compositions have been measured (Toulkeridis et al., 1994; 1998; 1999). Toulkeridis et al. concluded, however, that all three radiogenic isotopic systems were disturbed by later thermal events and provided little useful information on the eroded crust in the Barberton area. In this paper, we re-visit the Sm-Nd isotopic systematics of Fig Tree metasedimentary rocks and additionally explore their whole-rock Lu-Hf isotopic compositions using a larger dataset from core samples rather than samples from surface outcrops.

2. Geological overview of the eastern Kaapvaal craton

The Barberton granite-greenstone belt and the Ancient Gneiss Complex (Figure 1a) contain a rare, well-preserved 550 Ma (ca. 3.66-3.11 Ga) record of Archean crustal evolution. The construction of this part of the craton is mostly thought to be through subduction-accretion mechanisms with a major collision phase at ca. 3.23 Ga (de Wit et al., 1992; de Ronde and de Wit, 1994; Lowe, 1994; Lowe and Byerly, 1999; Moyen et al., 2006; Schoene and Bowring, 2010; de Wit et al., 2011; Furnes et al., 2012) though alternative models have been suggested; e.g. convective overturn of a dense upper crust and more buoyant middle crust (Van Kranendonk et al., 2009) or evolution of a plume-related oceanic plateau (Chavagnac, 2004).

In the subduction-accretion model, the eastern portion of the Kaapvaal craton is said to result from the assembly of at least two micro-continental blocks along NE-SW suture zones such as the Inyoka fault system (cf. Figure 1c). The Ancient Gneiss Complex and the northern and southern parts of the Barberton belt are often seen as possible building blocks sutured in the ca. 3.23 Ga convergent event (e.g. de Wit et al., 1992; Lowe, 1994; Schoene and Bowring, 2010). The tectono- and chrono-stratigraphy of the Ancient Gneiss Complex and the Barberton belt have been widely described and discussed in the literature since the 1970's (e.g. M. J. Viljoen and R. P. Viljoen, 1969; Hunter, 1970; Anhaeusser, 1973; Eriksson, 1980; de Wit, 1982; Kröner et al., 1989; Armstrong et al., 1990; Kröner et al., 1991; Kamo and Davis, 1994; Kröner and Tegtmeyer, 1994; Lowe and Byerly, 1999; Kröner, 2007; Schoene et al., 2008; Schoene and Bowring, 2010; de Wit et al., 2011; Furnes et al., 2013). Here, we present a brief geological overview and summarize a few observations and interpretations that provide the key for understanding the following discussion.

The Ancient Gneiss Complex contains the oldest rocks yet discovered in the Kaapvaal craton. It consists of deformed and metamorphosed tonalite-trondhjemite-granodiorites (TTGs) interlayered with amphibolites known as the Ngwane gneiss (3.66-3.50 Ga; Compston and Kröner, 1988; Kröner et al., 1989; Schoene et al., 2008; Zeh et al., 2011; Kröner et al., 2014) and by a series of metasedimentary and metavolcanic rocks called the Dwalile metamorphic suite (ca. 3.55 Ga; Kröner and Tegtmeyer, 1994) (Figure 1c). The two units are intruded by younger mafic-silicic banded orthogneisses and by a suite of tonalitic to granodioritic rocks (Schoene and Bowring, 2010). The Ancient Gneiss Complex is now separated from the Barberton greenstone belt by the 3.1 Ga-old Mpuluzi and Pigg's Peak granitic batholiths (e.g. Kamo and Davis 1994; cf. Figure 1c).

The Barberton granite-greenstone belt is a succession of tilted, folded and variably metamorphosed volcanic and sedimentary units, the Swaziland Supergroup, surrounded by orthogneiss complexes (e.g. Stolzburg and Steynsdorp complexes > 3.43 Ga; Kamo and Davis, 1994) and younger granitoid intrusions (e.g. Kaap Valley and Dalmien plutons at ca. 3.23 Ga; Armstrong et al., 1990; Kamo and Davis, 1994). The oldest unit of the Swaziland Supergroup, the 3.54-3.27 Ga-old Onverwacht group, consists of mafic and ultramafic rocks – komatiites and basalts mainly – with minor felsic volcanic and sedimentary rocks (see recent reviews by de Wit et al., 2011 and Furnes et al., 2013). The Onverwacht Group is overlain by the predominantly sedimentary Fig Tree (3.26-3.23 Ga; Kröner et al., 1991; Byerly et al., 1996) and Moodies Groups (3.23-3.11(?) Ga; Heubeck and Lowe, 1994) which consist of conglomerate, sandstone, shale, banded chert, banded iron formation and dacitic volcanic

rocks. In the subduction-accretion model, the Fig Tree and Moodies Groups could represent the fill of an evolving foreland basin fed by the erosion products of an orogenic complex (Lowe and Byerly, 1999).

3. Materials and methods

The study focuses on mudstones and sandstones recovered at different depths in two cores - BARB 4 and BARB 5 - drilled in the Mapepe formation of the Fig Tree Group. Drilling locations, simplified core logs and sampling depths are shown in Figure 1 and a detailed description of the samples is provided in Supplementary File A. Additionally, three drill core samples of chert from the Barberton area and fourteen outcrop samples of meta-igneous rocks from the Ancient Gneiss Complex from the Dwalile and Ngwane units were analyzed to see whether they could represent potential sources for the studied metasedimentary rocks (see white stars in Figure 1c and sample description in Supplementary File A).

We analyzed the trace element concentrations and the Sm-Nd-Lu-Hf isotopic compositions of the metasedimentary rocks from BARB 4 and BARB 5 drill cores, the three Buck Reef cherts and four meta-igneous rocks from the Ancient Gneiss Complex. The remaining ten meta-igneous rocks from the Ancient Gneiss Complex were analyzed for Sm-Nd isotopic compositions only. The detailed analytical procedure can be found in Supplementary File B. Major element concentrations of BARB 5 samples are available in Galic (2015). Samples preceded by "SWZ" were previously analyzed for trace and major elements by Hunter et al. (1984).

4. Results

4.1. Trace element concentrations

Measured trace element concentrations are reported in Supplementary Table A. They are shown normalized to the present-day upper continental crust composition (average UCC of Rudnick and Gao, 2014) and the post-Archean shale (average PAAS of Nance and Taylor, 1976 reported by Taylor and McLennan, 1985) in Figure 2. Metasedimentary rocks from the BARB 4 and BARB 5 drill cores share similar trace element distributions that resemble, to first order, the present-day upper continental crust (Figure 2a). Such concentrations are consistent with previously-analyzed siliciclastic rocks from the Fig Tree group (e.g. Hofmann, 2005). Trace element patterns are sub-parallel, which likely reflects a dilution effect by variable amounts of silica and/or carbonate. The samples show low concentrations

of incompatible elements relative to present-day upper continental crust and post-Archean shale, with slightly more depletion in the more highly incompatible elements. This is illustrated by the average $(Pr/Yb)_{N,\ PAAS}$ ratio of 0.50 ± 0.20 (2s) calculated for all metasedimentary rocks, where $_{N,\ PAAS}$ denotes normalization to the post-Archean shale ratio. With the exception of a few outliers, the patterns show depletion of Sr and Pb, and enrichment of Ba, Cr, Co and Ni. When normalized to post-Archean shale (Figure 2d), most samples have positive Eu anomalies, but no significant Ce anomalies. A few samples, one in particular (i.e. Ca-rich BARB 5-102.68) shows strong positive La and Eu anomalies ($(La/La^*)_{N,PAAS} = (La/(3Pr-2Nd))_{N,PAAS} = 1.5$; $(Eu/Eu^*)_{N,PAAS} = (Eu/(0.5Sm+0.5Gd))_{N,PAAS} = 1.8$) together with a superchondritic Y/Ho ratio of 51.2 (Figure 2b) that is a typical feature of seawater precipitates (Bau, 1996; Bolhar et al., 2004).

The three chert samples are distinguished from the detrital sediments by low concentrations in almost all trace elements, up to a hundred to a thousand times less abundant than the present-day upper continental crust for Cs, Rb, Ba, Th, Sr, Zr, Hf and Ti (Figure 2b). The chert breccia is generally more REE-rich (ΣREE = 41.8 ppm) than the black chert (ΣREE = 3.5 ppm), itself more enriched in REE than the translucent chert (ΣREE = 0.3 ppm). All cherts show strong depletions in the more highly incompatible elements and thus low $(Pr/Yb)_{N,PAAS}$ ratios (i.e. 0.17, 0.22 and 0.04 for the chert breccia, the black chert and the translucent chert, respectively; Figure 2e). The absence of a negative Ce anomaly, the presence of a positive Eu anomaly and the magnitude of depletion in the incompatible elements are typical of Archean cherts and banded iron formations (e.g. Bolhar et al., 2004; Hofmann, 2005; Bau and Alexander, 2009; Thurston et al., 2012; Ledevin et al., 2014).

As can be expected, the four samples that we analyzed from the Ancient Gneiss Complex show different trace element patterns as a function of their lithology (Figure 2c-2f). The Ngwane gneiss is the most enriched in Th, U, Nb, Ta, REE, Zr, Hf and Ti but also the most depleted in transition metals such as V, Cr, Co, Ni, Cu, Zn (Figure 2c). It has a LREE-depleted pattern and a slightly negative Ce anomaly relative to PAAS (Figure 2f). By contrast, the trace element distribution of the Dwalile basalt is almost the opposite with its very low concentrations in Th, U, Nb, Ta, REE, Zr, Hf and Ti and its strong enrichment in Cr, Co and Ni relative to present-day upper continental crust. Finally the two amphibolites share similar trace element patterns that resemble present-day upper continental crust and PAAS compositions. The two samples have a positive Eu anomaly relative to PAAS.

4.2. Sm-Nd and Lu-Hf isotopic compositions

Neodymium and Hf isotopic compositions are reported in Table 1 together with $^{147}Sm/^{144}Nd$ and $^{176}Lu/^{177}Hf$ ratios determined by isotope dilution. Also shown are initial isotopic compositions calculated at the sediment deposition age (i.e. 3.23 Ga) relative to the chondritic uniform reservoir (CHUR) using the reference values of Bouvier et al. (2008). Metasedimentary rocks from BARB 4 and BARB 5 show only a small range in $^{147}Sm/^{144}Nd$ ratios (average $^{147}Sm/^{144}Nd = 0.133 \pm 0.020$ (2s)) but variable $^{176}Lu/^{177}Hf$ ratios ($0.0063 < ^{176}Lu/^{177}Hf < 0.0437$). In a consistent way, their Nd isotopic compositions recalculated at 3.23 Ga span a small range of values ($-2.0 < \varepsilon_{Nd\ (t=3.23Ga)} < +1.7$) while their $\varepsilon_{Hf\ (t=3.23Ga)}$ are extremely variable ($-1.5 < \varepsilon_{Hf\ (t=3.23Ga)} < +13.1$), reaching Hf isotopic compositions even more radiogenic than that of the depleted mantle (calculated, as a simple approximation, at 3.23 Ga following a linear evolution from a chondritic composition at 4.55 Ga to a present-day extreme MORB value of $\varepsilon_{Hf\ (0)} = +20$; i.e. $(^{176}Hf/^{177}Hf)_{MORB,\ t=0} \sim 0.283350$).

Chert samples have generally higher $^{147}Sm/^{144}Nd$ ratios than the metasedimentary rocks from BARB 4 and BARB 5 ($^{147}Sm/^{144}Nd = 0.1437, 0.2893, 0.1796$ for the black chert, translucent chert and chert breccia, respectively). More importantly, they are characterized by extremely high $^{176}Lu/^{177}Hf$ ratios, up to a 100 times higher than common rocks ($^{176}Lu/^{177}Hf = 0.1843, 0.1253, 1.3324$ for the black chert, translucent chert and chert breccia, respectively). The high Lu/Hf ratios are consistent with their trace element patterns that show strong depletion in LREE and Hf relative to HREE (Figure 2b and 2e). Cherts share similar $\varepsilon_{Nd\ (t=3.23Ga)}$ with BARB 4 and BARB 5 metasedimentary rocks ($\varepsilon_{Nd\ (t=3.23Ga)} = -1.0, -0.1, -0.4$ for the black chert, translucent chert and chert breccia, respectively). Hf isotopic compositions recalculated at 3.23 Ga for the cherts are extremely radiogenic ($\varepsilon_{Hf\ (t=3.23Ga)}$ from +23 to +72) even though these values are associated with large uncertainties of up to 15ε_{Hf} units as explained at the end of Supplementary File B.

Rocks from the Ancient Gneiss Complex have variable $^{147}Sm/^{144}Nd$ (0.0898 to 0.2068; n=14) and $^{176}Lu/^{177}Hf$ ratios (0.0075 to 0.0270; n=4). Since the meta-igneous rocks were analyzed to see whether they could be the parent sources of the Fig Tree sediments, we report their initial Nd and Hf isotopic compositions recalculated at the sediment deposition age (i.e. 3.23 Ga) in Table 1. Initial Nd isotopic compositions recalculated at sediment deposition age span a

relatively large range ($\varepsilon_{Nd\ (t=3.23Ga)}$ = -3.4 to +2.0, n=14), just like their initial Hf isotopic compositons $\varepsilon_{Hf\ (t=3.23Ga)}$ values ($\varepsilon_{Hf\ (t=3.23Ga)}$ = -2.5 to +2.5, n=4). The Dwalile and Ngwane units share similar $\varepsilon_{Nd\ (t=3.23Ga)}$ averaging -1.0 ± 1.4 (1s, n=14) and -1.0 ± 1.6 (1s, n=4), respectively.

5. Discussion

5.1. Classification of metasedimentary rocks from BARB 4 and BARB 5 drill cores

The major and trace element composition of mature detrital sediments is mainly controlled by sedimentary processes, in particular mineral sorting (or hydrodynamic sorting) that occurs during sediment transport. Sorting during long transportation favors the formation of coarse-grained sediments enriched in quartz and heavy minerals while fine-grained sediments tend to be enriched in phyllosilicates such as clays (see for example Garzanti et al., 2011; Lupker et al., 2011). BARB 4 and BARB 5 sandstones contain limited amounts of detrital quartz (usually <10%) and instead consist mainly of angular and unsorted lithic clasts (>90%) (cf. Supplementary File A for the petrographic description of the samples). This composition reflects both incomplete weathering and short sediment transport distances, indicating that the geochemistry of the studied Archean sediments is not controlled by simple mineral sorting effects and cannot be understood using the reasoning applied to mature sediments. To understand which processes controlled the chemical composition of the samples, we performed a principal component analysis (PCA) using both major and trace element concentrations normalized to their standard deviations. The PCA results show that the first two principal components (PC1 and PC2) explain ~70% of the total variance in chemical composition. Loading factors for PC1 and PC2 are shown in Figure 3 (purple arrows) together with scores obtained for each sample in the new coordinate system (i.e. circles and squares in Figure 3). In detail, 56% of the total variance is explained by PC1, which is defined by positive correlations with Al_2O_3, TiO_2, K_2O, Na_2O, P_2O_5 and all trace elements but Cu. Principal component 2 (PC2) explains ~13% of the total variance and is defined by relatively high weights from CaO, MnO, MgO, FeO_T, Sr, Y and a few MREE, but negative correlation with SiO_2. Given the loading factors, we suggest that variations along PC1 reflect variable proportions of chemical sedimentary components (negative scores) and crustal detritus (positive scores). Variations along PC2 differentiate two different types of chemical sedimentary components and reflect variable proportions of Ca-, Fe-rich phases (positive

scores) and Si-rich phases (negative scores). Petrographic observations of the samples indicate that the Ca-, Fe-rich phases could be secondary or primary carbonate, iron oxide and/or pyrite while Si-rich phases correspond to secondary silica, detrital quartz, chert clasts and/or clasts of silicified rocks. Based on their scores, we differentiate three groups of samples in Figure 3:

(1) Samples that positively contribute to PC1 (gray points in Figure 3) can be classified as "crustal detritus-rich sediments".
(2) Samples that negatively contribute to PC1 but positively contribute to PC2 (dark pink points in Figure 3) can be classified as "Ca-, Fe-rich samples".
(3) Samples that negatively contribute to PC1 and negatively contribute to PC2 can be classified as "Si-rich samples" (pale pink points in Figure 3).

Our classification of metasedimentary rocks from PCA results is based on chemical compositions that can be used to explain the samples' Nd-Hf isotopic systematics. In the following discussion, the isotopic compositions of each group are considered separately to investigate different aspects of the Archean such as the formation and evolution of the crust or the prevailing environmental conditions. Note that the PCA method can be more generally applied to classify any type of sediment and/or screen for outliers prior to the interpretation of isotopic data.

5.2. The Archean crust of Barberton from detrital sedimentary rocks

5.2.1. Robustness of Lu-Hf and Sm-Nd isotopic compositions

The studied metasedimentary rocks from the BARB 4 and BARB 5 drill cores are largely detrital (i.e. sandstone and mudstone), but their petrography and chemical composition indicate that they contain a significant amount of chemical precipitates, such as the Ca-, Fe-, Si-rich phases identified in thin sections and by the PCA (cf. Figure 3). While some of the chemical sedimentary components are likely primary, some of these phases are clearly secondary, meaning that they formed after the deposition of the sediments, so that they may have overprinted the "truly-detrital" signature of the sediments. Toulkeridis et al. (1994; 1998; 1999) reached this conclusion following their study of the metasedimentary rocks from the Fig Tree group. They highlighted the resetting of Rb-Sr, Sm-Nd and Pb-Pb isotopic compositions by post-depositional events at ~2.6 and ~3.1 Ga, particularly in Fig Tree carbonates and greywackes. To minimize this issue, we chose to focus on metasedimentary rocks classified as "crustal detritus-rich sediments" only and evaluate whether their isotopic

compositions can be used to study the nature and age of the eroded crust in the Barberton area during the Paleoarchean period.

In igneous rocks, one can easily assess whether the Sm-Nd and Lu-Hf isotopic systematics of cogenetic samples or minerals have been perturbed after their crystallization by plotting the data on isochron diagrams (cf. Supplementary File C for an example with the meta-igneous rocks from the Ancient Gneiss Complex). This approach is not as simple for sedimentary rocks. Sedimentary rocks are mixtures of erosion products derived from different sources that are often not cogenetic, and hence do not share the same initial isotopic compositions. For example, a shale and a sandstone formed at the same time may contain variable proportions of juvenile mafic rock and recycled felsic crust (cf. Garçon and Chauvel, 2014). If the isotopic compositions of the shale and the sandstone are significantly different at the sediment deposition time, and the range of parent-daughter ratios is relatively small, then the slope defined by the data on an isochron diagram has no age significance because it is dominated by isotopic differences inherited from different, unrelated source rocks. By contrast, if all components of the sediment have similar isotopic compositions at the time of deposition, but different parent-daughter ratios - either due to their initial nature or because the ratios were changed by processes involved in sediment transportation/deposition - then the situation resembles the isochron case and the slope in the isochron diagram corresponds to an age that is close to the sediment deposition age. The extent to which the sediment isotopic heterogeneity at deposition age propagates into isochron age inaccuracy can be quantitatively evaluated. In brief, the variation of slope (dα), or the variation of age (dt) produced by sediment heterogeneity on the isochron age can be defined, for the Lu-Hf isotopic system, as:

$$dt = \frac{1}{\lambda} * \frac{d\alpha}{e^{\lambda t}} \qquad with \qquad d\alpha = \frac{\left(\frac{^{176}Hf}{^{177}Hf}\right)_{max,t} - \left(\frac{^{176}Hf}{^{177}Hf}\right)_{min,t}}{\left(\frac{^{176}Lu}{^{177}Hf}\right)_{max,0} - \left(\frac{^{176}Lu}{^{177}Hf}\right)_{min,0}}$$

where λ is the radioactive decay constant, $\left(\frac{^{176}Hf}{^{177}Hf}\right)_{max,t} - \left(\frac{^{176}Hf}{^{177}Hf}\right)_{min,t}$ the variability of isotopic compositions at sediment deposition age (t) and $\left(\frac{^{176}Lu}{^{177}Hf}\right)_{max,0} - \left(\frac{^{176}Lu}{^{177}Hf}\right)_{min,0}$ is the range of variability of parent-daughter ratios measured at present-day.

This calculation shows that a range of ~2ε units in the isotopic composition of sediments deposited at 3.23 Ga coupled to parent-daughter ratios varying between 0.11 and 0.14 for $^{147}Sm/^{144}Nd$ and 0.006 and 0.020 for $^{176}Lu/^{177}Hf$, as for the crustal detritus-rich sediments (Figure 4) will significantly perturb the slope of the array in an isochron diagram, and hence

the age defined by this trend. Even such minor sediment heterogeneity will generate an age variation (dt) of ±0.5 Ga and ±0.2 Ga for the Sm-Nd and Lu-Hf isotopic systems, respectively. This effect must be taken into account when evaluating sediment isotopic data.

In Figure 4, crustal detritus-rich sediments define linear trends whose slopes correspond to Sm-Nd and Lu-Hf ages of 3.13 ± 0.48 Ga and 3.37 ± 0.38 Ga, respectively. The large age uncertainties and the high MSWD of the correlations reflect the scatter of the data around the best-fit lines, which can be generated by sediment isotopic heterogeneity at deposition age as discussed above and/or an open system behavior after sediment deposition. Here, both the Sm-Nd and Lu-Hf ages are consistent, within error, with the sediment deposition age of the Fig Tree group (i.e. 3.23-3.26 Ga). This means that (1) the two isotopic systems have not been significantly perturbed in the crustal detritus-rich sediments since their deposition age, and (2) their isotopic composition was relatively homogenous when they formed at 3.23-3.26 Ga. Assuming that the two isotopic systems were not disturbed after 3.23 Ga thus implies that the isotopic composition of the crustal detritus-rich sediments at deposition age ranged between -1.6 and +0.1 for ε_{Nd}, with an average at -0.9 ± 1.0 (2s) and between -0.8 and +4.0 for ε_{Hf}, with an average at +0.6 ± 3.2 (2s).

5.2.2. Sediment provenance and composition of the eroded crust

5.2.2.a. What are the sources of the sediments?

The Nd-Hf isotopic compositions of crustal-detritus rich sediments are shown in Figure 5a together with the composition of their potential sources in the Barberton area and the Ancient Gneiss Complex. Both Nd and Hf isotopic compositions of the sediments are consistent with a mixture of mafic and felsic sources, as suggested by previous studies (Condie et al., 1970; Toulkeridis et al., 1999; Hofmann, 2005; Drabon et al., 2014). However, the large scatter in compositions of the potential source rocks, and the lack of Hf isotopic data, in particular for young felsic units, precludes further inferences about the nature of the eroded terranes from Figure 5a. Furthermore, sedimentary processes fractionate the Lu-Hf more easily than the Sm-Nd isotopic system mainly because Lu is not hosted in the same minerals as Hf whereas Sm and Nd are usually carried by the same phases (Patchett et al., 1984; McLennan, 1989; Garçon et al., 2013; Garçon et al., 2014; Bayon et al., 2015). The focus is thus on the Sm-Nd isotopic system (Figure 5b and 5c) to constrain both the sources of the sediments and the composition of the eroded crust.

The first important conclusion that can be drawn from Figure 5b and 5c is that very few igneous rocks from the Barberton area or the Ancient Gneiss Complex share the Nd isotopic

compositions of the Fig Tree metasedimentary rocks. This could mean that the source of the sediments has not been sampled, or more likely that the sediments do not derive from the erosion of a unique lithological source. The Nd isotopic compositions of the sediments are indeed well explained as mixtures of mafic-ultramafic and felsic sources derived solely from the Barberton area (Figure 5b). Contributions from both young and old felsic rocks are needed to account for the most unradiogenic Nd isotopic compositions. This requires that the sediments were sourced from at least three distinct units from the Barberton area. Rocks from the Ancient Gneiss Complex alone are not radiogenic enough to account for the entire range of Nd isotopic compositions measured in Fig Tree metasedimentary rocks (cf. Figure 5c). We do not exclude a contribution from rocks from the Ancient Gneiss Complex, but suggest that the more likely sources of the Fig Tree sediments are mafic-ultramafic and felsic rocks from the Onverwacht group and maybe the surrounding intrusions of the Barberton area (Figure 5b). This interpretation is in agreement with previous petrographic studies describing Mapepe detrital sediments as mixtures of terrigenous debris derived from the uplift and erosion of the Onverwacht Group, felsic volcanic rocks and the previously formed units of the lower Fig Tree Group (e.g. Nocita, 1989; Lowe and Nocita, 1999; Drabon et al., 2014).

5.2.2.b. Proportion of mafic vs. felsic material in the sediments and the eroded crust

Figure 5b also provides important information regarding the relative proportions of mafic vs. felsic material in the sediments and in the eroded crust. The Sm-Nd isotopic systematics indicate that Fig Tree sediments are made up of 30 to 65% mafic erosion products. Most samples, and all the mudstones, contain ~50-65% mafic material, while two sandstones (the outliers identified in Figure 5b) contain only ~30% mafic material and ~70% felsic erosion products. The contrasting provenance of fine and coarse-grained sediments is not surprising and has been previously observed in modern sedimentary systems. Garçon and Chauvel (2014) showed that mafic volcanic rocks tend to be over-represented in fine-grained sediments and under-represented in coarse-grained ones because mafic-ultramafic volcanic rocks yield more clays and dissolved species than their felsic equivalents. Since the proportions of mafic materials are not quantitatively transferred from sources to sediments, those deduced from mudstone isotopic compositions overestimate the abundance of mafic contributions compared to what was exposed at the surface. Conversely, proportions of felsic material in the two outlier sandstones are overestimated compared to their likely relative abundances in the terrane eroding to provide the material deposited in the sediments. Hence, we suggest that the composition of the eroded crust was between the endmember proportions

indicated by the mud- and sandstones, and was likely made up of near-equal proportions of mafic and felsic rocks (i.e. 50:50).

Another way to constrain the proportion of mafic vs. felsic rocks exposed in the Barberton area at ~ 3.2 Ga is to focus on the $^{147}Sm/^{144}Nd$ ratios of the sediments. Due to their different degrees of incompatibility, Sm and Nd are partitioned differently by differentiation processes within the crust. This generates a range of $^{147}Sm/^{144}Nd$ ratios in crustal rocks that is, in part, related to the rock's SiO_2 content, except for Si-undersaturated rocks, but these are essentially absent from the Paleoarchean record. Inspired by the recent studies of Tang et al. (2016) and Dhuime et al. (2015), we compiled about 3400 analyses from the GEOROC database to explore the precise inverse correlation between the $^{147}Sm/^{144}Nd$ ratios of crustal rocks and their SiO_2 content (Figure 6, see caption for more details). This correlation has been known since the early days of the application of the Sm-Nd system to crustal rocks but has not been exploited quantitatively. The compilation excluded settings like ocean islands and continental rifts because their $^{147}Sm/^{144}Nd$ ratios are dominated by mantle source enrichment which overwhelms the effect on Sm/Nd of crustal differentiation, the process we want to explore in this study. Figure 6 shows that the relationship between $^{147}Sm/^{144}Nd$ ratio and SiO_2 content of crustal rocks is well defined and, more importantly, very consistent with the values reported for the present-day average upper continental crust (see red box in Figure 6). Assuming that alteration and hydrodynamic sorting do not significantly fractionate Sm from Nd in sediments (McLennan, 1989; Garçon et al., 2013; Bayon et al., 2015), the average $^{147}Sm/^{144}Nd$ ratios of crustal detritus-rich mud- and sandstones can be interpolated on the fitted curve of Figure 6 to estimate the average SiO_2 content in the eroded Archean crust. This gives an average SiO_2 concentration of 60.5 ± 2 wt.% (blue box in Figure 6), showing that the portion of Archean upper crust that eroded to provide the sedimentary material in the Barberton area was significantly more mafic than the present-day upper continental crust (Rudnick and Gao, 2014). Note that the interpolated SiO_2 content is entirely consistent with previous interpretations from Figure 5b since a mixture of 50% of mafic rocks (SiO_2 = ~50 wt.%) and 50% of felsic rocks (SiO_2 = ~70 wt.%) results in an average SiO_2 content of 60 wt.%.

The high proportion of mafic component in the sedimentary source area is also well reflected by the trace element signature of the crustal-detritus-rich sediments, in particular the strong enrichments in Cr, Co and Ni (see Figure 2a). These elements are typical of mafic-ultramafic rocks (cf. trace element pattern of the Dwalile basalt in Figure 2c) and are present in far lower concentrations in modern sediments that are derived from the erosion of a more felsic upper crust (Taylor and McLennan, 1985; Garçon and Chauvel, 2014; Gaschnig et al., 2014;

Gaschnig et al., 2016). Ratios of immobile trace elements such as Th/Sc and La/Yb, shown in Figure 7 and often used as provenance tracers in sediments, further support the above interpretations. Due to their high proportion of mafic components, the crustal detritus-rich sediments from Barberton have significantly lower La/Yb and Th/Sc ratios than the post-Archean shale (PAAS) and modern upper crust (Figure 7). Their trace element composition is compatible with a mixture of detritus derived from local mafic-ultramafic and felsic rocks; the two sandstones being the more enriched in felsic erosion products. Note that the relative proportions deduced from trace element ratios (Figure 7) do not agree with those obtained from their $^{147}Sm/^{144}Nd$ ratios (Figure 6). This is because mixing proportions calculated using trace element ratios are largely under-constrained due to the paucity and scattering of the data available in the literature for felsic rocks from the Barberton area (cf. Figure 7). Further analyses of felsic volcanic, volcaniclastic and plutonic rocks from the Barberton area are required to resolve this inconsistency.

5.2.2.c. Was the Archean crust really more mafic than today?

The mafic composition inferred above for the crust eroded in the Barberton area implies that a smaller proportion of differentiated, sialic crustal components was present in the sedimentary source area at ~3.2 Ga. Perhaps differentiated silicic crustal rocks were not proximal to the sedimentary basin. More likely, a larger portion of the surface was covered by subaerial mafic volcanic rocks because the studied sediments sampled the crust before the big wave of plutonism that produced the 3.1 Ga granitoids that dominate the present-day exposure of the eastern Kaapvaal region (cf. Figure 1). A growing number of studies now converge to the idea that Archean upper crust had a more mafic composition than modern upper continental crust. This was first suggested by the pioneering studies of Taylor and McLennan (1985) and Condie (1993) showing that both Archean cratonic shales and sediments from greenstone belts derived from more mafic sources than post-Archean sediments. In particular, Condie's results on cratonic shales imply that the mafic composition of the upper Archean crust was not restricted to greenstone belt-tectonic setting only. Our results and the more recent studies of Gaschnig et al. (2016) and Tang et al. (2016) using larger datasets in time and space, clearly strengthen this view at a global scale.

The depth in the crust to which the high proportion of mafic rocks extends however is difficult to estimate. Most of the above studies, including ours, rely on sediment that samples the surface crust exposed to weathering, which may not be representative of bulk upper Archean crust composition. In South Africa, geoelectric and gravity data (De Beer et al.,

1988) suggest that the Barberton belt, in particular the mafic-ultramafic Onverwacht group, extends to a minimum depth of 4 km and a maximum of 8 km. Assuming that the Archean upper crust was 10 to 15 km-thick (Rudnick and Fountain, 1995), the mafic composition may be representative of nearly half of the upper Archean crust. Deeper in the Kaapvaal crust, seismic studies indicate that the middle and lower portions of the crust are felsic to intermediate in composition, excluding the Bushveld area (James et al., 2003; Nair et al., 2006; Youssof et al., 2013). Felsic to intermediate deep crust is also inferred from seismic data beneath the Paleo- to Neoarchean terranes of the Northern Canadian Shield (Thompson et al., 2010) and the Zimbabwe craton (Nair et al., 2006). By contrast, geophysical data suggest the presence of a thick mafic crust beneath Indian terranes that formed prior to 2.6 Ga (Das et al., 2015). A more mafic mid- to lower crust is more in line with the conclusions of Rudnick and Fountain (1995), Keller and Schoene (2012) and Dhuime et al. (2015). To summarize, studies based on sediments show clearly that Archean continents had more mafic rock exposure than post-Archean continental crust. To which depth in the crust this higher proportion of mafic rocks extended is still unclear and needs to be further investigated to affirm that the bulk Archean crust was more mafic than today.

5.2.3. Crustal growth history and building of the Eastern Kaapval craton

Nd and Hf model ages, also called crustal residence ages, are useful to estimate the average extraction age of rocks from their mantle sources, often assumed to be the depleted mantle. Here we calculate the model ages for the crustal detritus-rich sediments in order to evaluate the average age of the Archean crust that was eroded in the Barberton area (details about the calculations are provided in the caption of Figure 8). Figure 8 shows that most crustal detritus-rich sediments converge towards roughly one Nd and Hf model age of ~3.5-3.6 Ga. Hf model ages are slightly younger than Nd ages for a given sediment because they were calculated in one stage, using the Hf isotopic compositions and the $^{176}Lu/^{177}Hf$ ratios of sediments as if they were representative of those of the eroded crust. However, sedimentary processes, in particular mineral sorting, can modify Lu-Hf isotopic systematics, which may bias the calculated Hf model ages towards slightly younger values. By subtracting the deposition age of the sediments from the model ages, we calculate that the eroded Archean terrane was on average ~300-400 Ma older than the deposition age of the sediments at ~3.2 Ga. This interval is much shorter than the average crustal residence age of the present-day upper crust (i.e. 1.8 ± 0.4 Ga; Jacobsen, 1988) but corresponds, as today, to ~1/3 of the age of the Earth at sediment deposition time. The 1/3 ratio suggests that a relatively large proportion

of older crust was exposed at the surface and likely remelted during the major collision event that contributed to building the eastern Kaapvaal craton at ca. 3.23 Ga.

The importance of intracrustal reworking in the making of the eastern Kaapvaal craton has been highlighted by several studies, in particular Schoene et al. (2009) based on Sm-Nd isotopic compositions of 3.66 to 2.70 Ga-old granitoids and Zeh et al. (2009; 2011; 2013) based on Hf isotopic compositions of zircons. To see whether the Barberton sediment data are consistent with the crustal growth history depicted by previous studies, we report the initial epsilon Nd-Hf of crustal detritus-rich sediments as a function of time in Figure 9, together with published Nd-Hf isotopic compositions of whole-rocks from the Barberton and Ancient Gneiss complex areas and Hf isotope data of detrital zircons from the Fig Tree and Moodies units. The general decreasing trend towards more negative epsilon values in younger magmas that is particularly well-defined by the zircon data in Figure 9b confirms that most felsic magmas formed after 3.3 Ga inherited a component from an older felsic crust. Except for the two 3.23 Ga samples with radiogenic Hf isotopic compositions, the crustal detritus-rich sediments consistently plot within the general decreasing trend, indicating that intracrustal remelting of older crust was not restricted to just a few igneous bodies but was sufficiently widespread and important to be recorded by sediments draining large continental areas at 3.23 Ga. Nd-Hf data (Figure 9) indicate that the old remelted felsic crust could have been extracted from the depleted mantle at 3.5-3.6 Ga, which is consistent with the formation ages and the Nd-Hf isotopic compositions of some of the oldest rocks from the Barberton area and the Ancient Gneiss Complex (Figure 9).

5.3. The Archean environment as seen by chemical sedimentary components

5.3.1. Cherts and silicification: effect on Lu-Hf isotopic systematics of sedimentary rocks

Nd and Hf isotopic compositions of Si- and Ca-, Fe-rich sediments can provide insights on the Archean environment because they are rocks formed under Archean surface condition. Figure 10 shows ε_{Nd} and ε_{Hf} of Si and Ca-, Fe-rich sediments recalculated at 3.23 Ga, the deposition age of the sediments. The most striking feature is the extremely radiogenic ε_{Hf} values of the Si-rich sediments, up to +11, which is much higher than the predicted composition of the depleted mantle at 3.23 Ga as shown in Figure 10. These unusually high ε_{Hf} values could be theoretically explained by a post-depositional disturbance of sufficient intensity to decrease the Lu/Hf ratio or affect the Hf isotopic composition of the sediments

after their deposition. However, the studied samples have been subjected to only low-grade metamorphic conditions (up to greenschist facies) and silicification is such a low-temperature process (<200°C) that it seems unlikely that it would have affected Hf isotopic compositions. More importantly, the Si-rich sediments have a small range of $\varepsilon_{Nd\ (t=3.23\ Ga)}$ values that strongly resembles those of the crustal detritus-rich sediments (Figure 10). In the Sm-Nd isochron diagram (Figure 11), the Si-rich sediments define a trend whose slope corresponds to an age of ~3.8 Ga, which is not well constrained due to limited range in Sm/Nd but clearly not reset by a later event. The last two observations suggest that the Sm-Nd isotopic system has not been significantly disturbed in Si-rich sediments after their deposition. Therefore, if the high $\varepsilon_{Hf\ (t=3.23\ Ga)}$ values result from a post-depositional disturbance, one needs to find a process able to significantly perturb Lu-Hf isotopic systematics but not Sm-Nd. This is, in our opinion, very unlikely.

The sediments classified as "Si-rich" are all sandstones, mostly coarse-grained and from the BARB 4 drill core (Table 1). Petrographic studies show that BARB 4 coarse-grained sandstones represent composites of common silicified rocks from the Barberton area and additionally contain a high amount of chert clasts (Drabon et al., 2014). The overabundance of chert clasts explains why these sediments have been classified as "Si-rich" by the PCA. We suggest that the presence of the chert clasts can also account for their extremely radiogenic initial Hf isotopic compositions. To test this hypothesis, we analyzed three chert samples (translucent chert, black chert and chert breccia) from the Buck Reef formation (3.42 Ga, Kröner et al., 1991) lying at the base of the Kromberg formation in the Onverwacht group. These cherts are older than the Fig Tree metasedimentary rocks and are thus good candidates for sources of the chert clasts in the studied sediments. Analyses of these cherts show that they have extremely low concentrations of most trace elements and higher Lu, Sm and Nd concentrations compared to Hf (see Figure 2b-2e) that translate into unusually high Lu/Hf ratios. The three cherts define linear trends in both the Sm-Nd and Lu-Hf isochron diagrams (Figure 12). The slopes of these trends yield ages of ~3.3 Ga, which are consistent within error with the estimated age of formation of the Buck Reef cherts at ~3.42 Ga (Lowe and Byerly, 1999).

The present-day Hf isotopic compositions of the cherts are among the most radiogenic compositions ever measured for terrestrial rocks, reaching $^{176}Hf/^{177}Hf_{\ (t=0)}$ ratios of ~0.37, that is, a remarkable $\varepsilon_{Hf\ (t=0)}$ of +2931, and $^{176}Lu/^{177}Hf$ ratios up to ~1.33 (Figure 12). The Lu/Hf

598 ratios of the three cherts are so elevated that, at 3.23 Ga, only a few hundred million years
599 after their formation, they would have developed extremely radiogenic Hf isotopic
600 compositions ($\varepsilon_{Hf\ (t=3.23Ga)}$ = +23 to +72; Table 1 and Figure 10). Their Nd isotopic
601 compositions at 3.23 Ga are nonetheless close to chondritic values and very similar to all
602 other metasedimentary rocks from the BARB 4 and BARB 5 drill cores (Table 1; Figure 10).
603 Given the highly unusual Nd-Hf isotopic compositions of cherts, we suggest that the presence
604 of old chert clasts and silicified lithic grains in the Si-rich sediments explain their unusually
605 high $\varepsilon_{Hf\ (t=3.23Ga)}$ but normal $\varepsilon_{Nd\ (t=3.23Ga)}$. Binary isotopic mixing between cherts and crustal
606 detritus-rich sediments is consistent with this interpretation. Figure 10 shows that the
607 proportion of silicified clasts must be as high as 90% to account for the radiogenic Hf isotopic
608 compositions of Si-rich sediments, proportions that are in agreement with measured SiO_2
609 contents and petrographic observations showing that the Mapepe sandstones are commonly
610 made up of ~90% of lithic silicified/chert clasts.
611 This result potentially has more global implications as it could help explain the decoupling of
612 Nd and Hf isotopic compositions seen in other sedimentary rocks. Fig Tree sedimentary rocks
613 are highly silicified and represent an extreme case where cherts and silicified clasts constitute
614 up to 90% of the rock. The amount of chert clasts needed to significantly shift the bulk
615 sediment Hf isotopic composition however depends on the lapse of time between the
616 formation of the cherts and their erosion to form the sediments. The older the chert clasts, the
617 more radiogenic their Hf isotopic compositions are, the less chert clasts are needed to
618 significantly affect the bulk Hf isotopic composition of the sediment. The presence of 20% of
619 Archean cherts, such as sample B3-227-Ch3, in a modern sediment having the same
620 composition as the modern upper crust (i.e. $\varepsilon_{Hf\ (t=0)}$ = -13 and C_{Hf} = 5.3 ppm; Chauvel et al.,
621 2014) would for example shift the bulk Hf isotopic composition of the modern sediment by
622 about +6 ε units.

623

624 *5.3.2. Chemical sediments: proxies for Archean seawater compositions?*
625 The origin of cherts and other chemical sediments as primary or secondary precipitates is still
626 debated in the literature (e.g. Paris et al., 1985; Weis and Wasserburg, 1987; Lowe and
627 Byerly, 1999; Hofmann, 2005; Tice and Lowe, 2006; Rouchon and Orberger, 2008; Ledevin
628 et al., 2014). Discussing the formation of these chemical sediments in detail is beyond the
629 scope of this manuscript but we can evaluate whether the chemical precipitates have

preserved a seawater signal and can be used to provide insights on the Nd-Hf isotopic systematics of Archean seawater. Seawater and its chemical precipitates have typical trace element signatures that develop mainly in aqueous systems. This is because the behavior of trace elements in aqueous media is controlled not only by ion charge and radius as in most igneous rocks (charge and radius controlled i.e. CHARAC behavior) but additionally depends on chemical complexation, in particular the type of ligands and the electron configuration of the aqueous complexes (Bau, 1996). Typical features of seawater-like trace element signatures, as summarized by Bolhar et al. (2004) and Bau (1996), include superchondritic Y/Ho and Zr/Hf ratios (i.e. non-CHARAC ratios), positive La and Gd anomalies in post-Archean shale-normalized REE-Y diagrams, depletion in LREE and MREE relative to HREE, and low REE and HFSE concentrations. The Buck Reef cherts and most of the Ca-, Fe- rich sediments however have typical CHARAC-like Y/Ho and Zr/Hf ratios (Figure 13) and do not exhibit any particularly strong La or Gd anomalies (Figure 2d and 2e). This indicates that these chemical sediments likely did not precipitate from seawater and/or that the primary seawater-like signature is blurred by the presence of detrital particles (Bolhar et al., 2004); hence they cannot be used to study the Nd-Hf isotopic systematics of Archean seawater, at least not in a simple, straightforward way.

One sample from the BARB 5 drill core (sample BARB5-102.68) however has a very peculiar petrographic and chemical composition compared to other Ca-, Fe-rich metasedimentary rocks. This sample is mainly composed of carbonate grains and iron oxides at grain boundaries and has one of the strongest enrichments in Ca, Fe and Mg (CaO = 37.8 wt.%; FeO_T = 17.3 wt.%; MgO = 14.8 wt.%; Galic, 2015), but also a superchondritic Y/Ho ratio of ~51.2 (Figure 13), a positive La anomaly when normalized to post-Archean shale, and a depletion in LREE relative to HREE (Figure 2d). Sample BARB5-102.68 thus has the main features of a marine precipitate, suggesting that its REE-Y distribution, hence its Nd isotopic composition, has preserved a seawater-like signature. Note that the Zr/Hf ratio of this sample is chondritic (i.e. CHARAC behavior, see Figure 13), which may suggest that its Hf and/or Zr are not sourced from seawater or, alternatively, that seawater had a chondritic Zr/Hf ratio as suggested by Bau and Alexander (2009). The lack of Ce anomaly and the positive Eu anomaly (Figure 2d) are common features in Archean sediments (e.g. Bolhar et al., 2004; Hofmann, 2005; Bau and Alexander, 2009; Thurston et al., 2012) and can be taken as evidence for anoxic conditions and higher hydrothermal inputs to the ancient oceans (e.g. Fryer, 1977; Appel, 1983; Derry and Jacobsen, 1990). Interestingly, carbonate BARB5-

102.68 has the most radiogenic Nd isotopic composition of our dataset ($\varepsilon_{Nd\ (t=3.23Ga)}$ = ~ +1.7; Table 1; Figure 10). We acknowledge that the composition of the Archean oceans cannot be estimated from one sample, but we note that this ε_{Nd} value is compatible with Alexander et al.'s (2009) suggestion that bulk anoxic seawater had a relatively constant $\varepsilon_{Nd\ (t)}$ of approximately +1 to +2 during the Archean period. The radiogenic Nd isotopic composition of the Archean oceans may be accounted for by a combination of higher hydrothermal input and higher contribution of dissolved material derived from the weathering of juvenile mafic-ultramafic rocks (Kamber, 2010). The ε_{Nd} of the carbonate is indeed very similar to the average Nd isotopic composition of mafic-ultramafic rocks from the Barberton area (cf. Figure 5b), which could reflect their over-representation in seawater (cf. Dessert et al., 2003), just as they are over-represented in shale compared to sandstone (cf. section 5.2.2.b).

Acknowledgements

We thank P. Mason (Utrecht University, Netherland), A. Galic (Utrecht University, Netherland), D.R. Lowe (Stanford University, U.S.A.) and N. Drabon (Stanford University, U.S.A.) for letting us use their major element data and for helping on the description of the sample petrography; M. Ledevin (Institute for Planetary materials, Japan) for her description of the Buck Reef chert petrography; C. Chauvel (ISTerre, Grenoble University, France) and M. Boyet (Laboratoire Magmas et Volcans, France) for their constructive comments on the elemental and isotopic data. We also acknowledge the International Continental Scientific Drilling Program (ICDP) and are grateful to the associate editor Yuri Amelin and two anonymous reviewers who provided many helpful comments. This study was funded by the Carnegie Institution of Washington.

Table Caption

Table 1: Sm-Nd and Lu-Hf isotopic compositions of metasedimentary rocks from the Barberton area and meta-igneous rocks from the Ancient Gneiss Complex.

Duplicate stands for complete dissolution duplicate. s_N are in-run standard errors. Epsilon values are calculated relative to the present-day CHUR composition of Bouvier et al. (2008).

Figure Caption

Figure 1: The Barberton area and the Ancient Gneiss Complex.

(a) Location of the Kaapvaal craton in South Africa and Swaziland. (b) Legend of the geological map. (c) Geological map of the eastern Kaapvaal craton modified after Schoene et al. (2009) and Ledevin et al. (2014). Sampling locations of cherts from the Barberton area and meta-igneous rocks from the Ancient Gneiss Complex are indicated by white stars. (d) Simplified core logs of BARB 4 and BARB 5 drilled in the Mapepe formation of the Fig Tree group in the Barberton area. Sampling depths are indicated by white stars.

Figure 2: Trace element patterns

Left panels: trace element concentrations of (a) BARB 4 and BARB 5 metasedimentary rocks, (b) cherts and (c) meta-igneous rocks from the Ancient Gneiss Complex normalized to the present-day upper continental crust composition of Rudnick and Gao (2014). *Right panels:* REE + Y concentrations of (d) BARB 4 and BARB 5 metasedimentary rocks, (e) cherts and (f) meta-igneous rocks from the Ancient Gneiss Complex normalized to post-archean shale composition (PAAS; Nance and Taylor, 1976; Taylor and McLennan, 1985).
In panels (d), (e) and (f), Pm and Tm are shown to respect the slope of the REE pattern. The Rb concentration of the Dwalile basalt shown in (c) was below detection limits, hence we interpolated the pattern between Ba and Cs. Detection limit is defined as 3 times the number of counts/sec measured on blanks for one analytical sequence.

Figure 3: Results of the principal component analysis (PCA) of major and trace elements
The PCA allows the classification of metasedimentary rocks from BARB 4 and BARB 5 drill cores into three groups of samples: the crustal detritus-rich sediments (dark grey), the Ca-, Fe-rich sediments (dark pink) and the Si-rich sediments (light pink). Purple arrows are graphic representations of loading factors (i.e. weight of each variable on PC1 and PC2). The coordinates of each sample in the new PC1 vs. PC2 space (i.e. sample scores) are shown by squares (BARB 4) and circles (BARB 5).

Figure 4: Sm-Nd and Lu-Hf isochron diagrams for crustal-detritus rich sediments.
(a) Present-day $^{143}Nd/^{144}Nd$ ratios as a function of $^{147}Sm/^{144}Nd$ ratios. (b) Present-day $^{176}Hf/^{177}Hf$ ratios as a function of $^{176}Lu/^{177}Hf$ ratios. Shaded areas indicate 95% confidence level. Measurement errors are smaller than the symbol sizes.

Figure 5: Nd and Hf isotopic compositions of crustal detritus-rich sediments compared to their potential rock sources from the Barberton area and the Ancient Gneiss Complex.

(a) $\varepsilon_{Hf\ (t=3.23\ Ga)}$ as a function $\varepsilon_{Nd\ (t=3.23\ Ga)}$; (b) and (c) $\varepsilon_{Nd\ (t=3.23\ Ga)}$ as a function of $^{147}Sm/^{144}Nd$ ratios. Literature data are from Carlson et al. (1983), Kröner and Tegtmeyer (1994), Lahaye et al. (1995), Kröner et al. (1996), Chavagnac (2004), Clemens et al. (2006), Schoene et al. (2009), van Kranendonk et al. (2009), Furnes et al. (2012), Kröner et al. (2013), Puchtel et al. (2013), Kröner et al. (2014), Blichert-Toft et al. (2015) and Hoffmann et al. (2016). For the Barberton area, young felsic rocks include gneisses, tonalites and granodiorites from Nelspruit and Stentor basements, Kaap Valley and Nelshoogte plutons, and Vlakplaats area; old felsic rocks include a tonalitic dike (Komati formation) and felsic volcanics (Theespruit and Hooggenoeg formations) from the Onverwacht group together with gneisses and tonalite-granodiorites from Stolzburg and Steynsdorp terranes; mafic and ultramafic rocks are all from the Onverwacht group and include basalts, komatitic basalts, komatiites and a few gabbros from the Theespruit, Komati, Hooggenoeg, Kromberg, Mendon and Weltevreden formations. For the Ancient Gneiss Complex, young felsic rocks include gneisses, tonalites and granodiorites from the Usutu and Nhlangano suites; old felsic rocks include mostly tonalitic and grey gneisses from the Ngwane and Twasela units; mafic and ultramafic rocks include komatiites to basalts from the Dwalile suite. To our knowledge, no Hf isotopic data are available in the literature for young felsic rocks from the Barberton area and the Ancient Gneiss Complex as well as for mafic and ultramafic rocks from the Ancient Gneiss Complex. Colored stars show averages for each group of sources, averages that were used as endmembers in the isotopic mixtures. Ticks and numbers next to the mixing lines indicate the proportion of mafic-ultramafic materials in the mixtures (one tick every 10%). Error bars are fixed at ± 0.3 ε unit for Nd and ± 0.8 ε unit for Hf (see Supplementary File B). They are smaller than the symbol size for $^{147}Sm/^{144}Nd$ ratios. All epsilon values were recalculated relative to the CHUR composition of Bouvier et al. (2008).

Figure 6: Relationship between $^{147}Sm/^{144}Nd$ ratio and SiO_2 content of crustal rocks based on a compilation of 3397 volcanic and plutonic rocks from convergent margins, oceanic plateaus and Archean cratons.
Data are from the GEOROC database (http://georoc.mpch-mainz.gwdg.de/georoc). We used samples for which $^{147}Sm/^{144}Nd$ ratios were precisely determined by isotopic dilution only. Like Dhuime et al. (2015), black dots correspond to median $^{147}Sm/^{144}Nd$ ratios calculated for each 1 wt.% SiO_2 interval (error bars indicate 2 s.e.). The best fit to the data is shown by the black line. The gray shaded area indicates the 95% confidence interval. The range of

762 $^{147}Sm/^{144}Nd$ ratios and SiO_2 contents known for the present-day upper continental crust are
763 shown by the red box ($^{147}Sm/^{144}Nd$ = 0.1012-0.1193 after Chauvel et al. (2014) and references
764 therein; SiO_2 = 66.6 ± 2.4 (2s) wt.% after Rudnick and Gao (2014)). The blue box
765 corresponds to the average composition of the eroded Barberton crust that we estimated using
766 the average $^{147}Sm/^{144}Nd$ ratio of the crustal detritus-rich sediments from BARB 4 and BARB
767 5 drill cores. UCC stands for upper continental crust.
768
769 **Figure 7:** La/Yb and Th/Sc ratios of the crustal detritus-rich sediments compared to their
770 potential rock sources from the Barberton area (log-log scale).
771 Symbols and colors as in Figure 5. Data for mafic-ultramafic rocks (basalts and komatiites
772 from the Onverwacht group mainly) are from Furnes et al. (2012), Robin-Popieul et al.
773 (2012), and Puchtel et al. (2013). Data for felsic rocks include silicic metavolcaniclastic rocks
774 from the Theespruit Formation of the Onverwacht Group and plutonic rocks from the
775 Nelshoogte, Steynsdorp, Stolzburg, Theespruit, Kaap Valley and Dalmien plutons (Glikson,
776 1976; Kohler and Anhaeusser, 2002; Kleinhanns et al., 2003; Kröner et al., 2013). UCC
777 stands for upper continental crust (data from Rudnick and Gao, 2014) and PAAS for post-
778 Archean shale (data from Taylor and McLennan, 1985). Ticks and numbers next to the
779 mixing line indicate the proportion of mafic-ultramafic material in the mixtures (one tick
780 every 10%). Note the sinusoidal form of the mixing line due to the use of a log-log scale.
781 Measurement errors are smaller than the symbol sizes.
782
783 **Figure 8:** Nd and Hf model ages (or crustal residence ages) of crustal detritus-rich sediments.
784 Model ages were calculated in one stage assuming that the depleted mantle has linearly
785 evolved from a CHUR composition (Bouvier et al., 2008) at 4.55 Ga to a present-day
786 composition of $\varepsilon_{Nd\ (t=0)}$ = +8.2 and $\varepsilon_{Hf\ (t=0)}$ = +13.0 corresponding to the average composition
787 of MORB compiled from the petDB database (http://www.earthchem.org/petdb) and
788 additional data from C. Chauvel. Error bars are at ± 0.1 Ga to account for variations in the
789 depleted mantle compositions and uncertainties on measured ε_{Nd}, ε_{Hf}, $^{147}Sm/^{144}Nd$ and
790 $^{176}Lu/^{177}Hf$ ratios.
791
792 **Figure 9:** Temporal evolution of initial Nd and Hf isotopic compositions of whole-rocks and
793 detrital zircons from the Barberton area and the Ancient Gneiss Complex.

Whole-rock data are from the literature (see caption of Figure 5 for references). Hf data for detrital zircons are from Zeh et al. (2013). As in Figure 8, the depleted mantle composition is assumed to have linearly evolved from a chondritic composition at 4.55 Ga to the present-day average composition of MORB ($\varepsilon_{Nd\ (t=0)}$ = +8.2 ; $\varepsilon_{Hf\ (t=0)}$ = +13.0). The evolution of the 3.5 Ga and 3.6 Ga felsic crusts is calculated using a $^{147}Sm/^{144}Nd$ ratio of 0.11 and a $^{176}Lu/^{177}Hf$ ratio of 0.009, which correspond to the medians of the parent-daughter ratios of old felsic rocks from the Barberton area and the Ancient Gneiss Complex. All epsilon values are calculated relative to the CHUR composition of Bouvier et al. (2008).

Figure 10: Nd and Hf isotopic compositions of Fig Tree metasedimentary rocks and Buck Reef cherts at 3.23 Ga.
The field of composition for depleted mantle (DM; purple box) was calculated back at 3.23 Ga following a linear evolution from a chondritic composition at 4.55 Ga to present-day average and extreme MORB compositions. The black line represents the mixing curve between the chert breccia and the average composition of the crustal detritus-rich sediments. Ticks represent increments of 10% of chert in the mixture. Error bars are fixed at ± 0.3 ε unit for Nd and ± 0.8 ε unit for Hf, except for cherts for which the measurement errors on $\varepsilon_{Hf\ (t=3.23Ga)}$ are much higher (see Supplementary File B). All epsilon values are calculated using the CHUR composition of Bouvier et al. (2008).

Figure 11: Sm-Nd isochron diagram for Si-rich sediments.
Shaded areas indicate 95% confidence level. Measurement errors are smaller than the symbol sizes.

Figure 12: Sm-Nd and Lu-Hf isochron diagrams for Buck Reef cherts.
(a) Present-day $^{143}Nd/^{144}Nd$ ratios as a function of $^{147}Sm/^{144}Nd$ ratios. (b) Present-day $^{176}Hf/^{177}Hf$ ratios as a function of $^{176}Lu/^{177}Hf$ ratios. Measurement errors are smaller than the symbol sizes.

Figure 13: Plot of Y/Ho ratios vs. Zr/Hf ratios showing Barberton metasedimentary rocks and cherts as well as fields for seawater, hydrothermal vein, Fe-Mn crusts, and CHARAC

825 samples (i.e. samples for which the behavior of trace elements is controlled by their charge
826 and radius; CHarge And RAdius Controlled).
827 Figure modified from Bau (1996). Metasedimentary rocks and cherts from Barberton are
828 color-coded as in Figure 10.
829
830 **References**

831 Alexander B. W., Bau M. and Andersson P. (2009) Neodymium isotopes in Archean seawater
832 and implications for the marine Nd cycle in Earth's early oceans. *Earth and Planetary*
833 *Science Letters* **283**, 144–155.

834 Anhaeusser C. R. (1973) The Evolution of the Early Precambrian Crust of Southern Africa.
835 *Philosophical Transactions of the Royal Society* **273**, 359–388.

836 Appel P. (1983) Rare earth elements in the early Archaean Isua iron-formation, West
837 Greenland. *Precambrian Research* **20**, 243–258.

838 Armstrong R. A., Compston W., de Wit M. and Williams I. S. (1990) The stratigraphy of the
839 3.5-3.2 Ga Barberton Greenstone Belt revisited: a single zircon ion microprobe study.
840 *Earth and Planetary Science Letters* **101**, 90–106.

841 Bau M. (1996) Controls on the fractionation of isovalent trace elements in magmatic and
842 aqueous systems: evidence from Y/Ho, Zr/Hf, and lanthanide tetrad effect. *Contrib*
843 *Mineral Petrol* **123**, 323–333.

844 Bau M. and Alexander B. W. (2009) Distribution of high field strength elements (Y, Zr, REE,
845 Hf, Ta, Th, U) in adjacent magnetite and chert bands and in reference standards FeR-3
846 and FeR-4 from the Temagami iron-formation, Canada, and the redox level of the
847 Neoarchean ocean. *Precambrian Research* **174**, 337–346.

848 Bayon G., Toucanne S., Skonieczny C., André L., Bermell S., Cheron S., Dennielou B.,
849 Etoubleau J., Freslon N., Gauchery T., Germain Y., Jorry S. J., Ménot G., Monin L.,
850 Ponzevera E., Rouget M. L., Tachikawa K. and Barrat J. A. (2015) Rare earth elements
851 and neodymium isotopes in world river sediments revisited. *Geochimica et*
852 *Cosmochimica Acta* **170**, 17–38.

853 Belousova E. A., Kostitsyn Y. A., Griffin W. L., Begg G. C., O'Reilly S. Y. and Pearson N. J.
854 (2010) The growth of the continental crust: Constraints from zircon Hf-isotope data.
855 *Lithos* **119**, 457–466.

856 Blichert-Toft J., Arndt N. T., Wilson A. and Coetzee G. (2015) Hf and Nd isotope systematics
857 of early Archean komatiites from surface sampling and ICDP drilling in the Barberton
858 Greenstone Belt, South Africa. *American Mineralogist* **100**, 2396–2411.

859 Bolhar R., Kamber B. S., Moorbath S., Fedo C. M. and Whitehouse M. J. (2004)
860 Characterisation of early Archaean chemical sediments by trace element signatures. *Earth*
861 *and Planetary Science Letters* **222**, 43–60.

862 Bolhar R., Kamber B. S., Moorbath S., Whitehouse M. J. and Collerson K. D. (2005)
863 Chemical characterization of earth's most ancient clastic metasediments from the Isua

Greenstone Belt, southern West Greenland. *Geochimica et Cosmochimica Acta* **69**, 1555–1573.

Bouvier A., Vervoort J. D. and Patchett P. J. (2008) The Lu–Hf and Sm–Nd isotopic composition of CHUR: Constraints from unequilibrated chondrites and implications for the bulk composition of terrestrial planets. *Earth and Planetary Science Letters* **273**, 48–57.

Byerly G. R., Kröner A., Lowe D. R. and Todt W. (1996) Prolonged magmatism and time constraints for sediment deposition in the early Archean Barberton greenstone belt: evidence from the Upper Onverwacht and Fig Tree groups. *Precambrian Research* **78**, 125–138.

Carlson R. W., Hunter D. R. and Barker F. (1983) Sm–Nd age and isotopic systematics of the bimodal suite, ancient gneiss complex, Swaziland. *Nature* **305**, 701–704.

Chauvel C., Garçon M., Bureau S., Besnault A., Jahn B.-M. and Ding Z. (2014) Constraints from loess on the Hf–Nd isotopic composition of the upper continental crust. *Earth and Planetary Science Letters* **388**, 48–58.

Chavagnac V. (2004) A geochemical and Nd isotopic study of Barberton komatiites (South Africa): implication for the Archean mantle. *Lithos* **75**, 253–281.

Clemens J. D., Yearron L. M. and Stevens G. (2006) Barberton (South Africa) TTG magmas: Geochemical and experimental constraints on source-rock petrology, pressure of formation and tectonic setting. *Precambrian Research* **151**, 53–78.

Compston W. and Kröner A. (1988) Multiple zircon growth within early Archaean tonalitic gneiss from the Ancient Gneiss Complex, Swaziland. *Earth and Planetary Science Letters* **87**, 13–28.

Condie K. C. (1993) Chemical composition and evolution of the upper continental crust: contrasting results from surface samples and shales. *Chemical Geology* **104**, 1–37.

Condie K. C. and Hunter D. R. (1976) Trace element geochemistry of Archean granitic rocks from the Barberton region, South Africa. *Earth and Planetary Science Letters* **29**, 389–400.

Condie K. C., Macke J. E. and Reimer T. O. (1970) Petrology and geochemistry of early Precambrian graywackes from the Fig Tree Group, South Africa. *Geological Society of America Bulletin* **81**, 2759–2776.

Das R., Saikia U. and Rai S. S. (2015) The deep geology of South India inferred from Moho depth and Vp/ Vs ratio. *Geophys. J. Int.* 203, 910–926.

De Beer J. H., Stettler E. H., Plessis Du J. G. and Blume J. (1988) The deep structure of the Barberton greenstone belt: a geophysical study. *South African Journal of Geology* **91**, 184–197. Available at: b.

de Ronde C. and de Wit M. (1994) Tectonic history of the Barberton greenstone belt, South Africa: 490 million years of Archean crustal evolution. *Tectonics* **13**, 983–1005.

de Wit M. (1982) Gliding and overthrust nappe tectonics in the Barberton greenstone belt. *Journal of Structural Geology* **4**, 117–136.

de Wit M. J., Furnes H. and Robins B. (2011) Geology and tectonostratigraphy of the Onverwacht Suite, Barberton Greenstone Belt, South Africa. *Precambrian Research* **186**, 1–27.

de Wit M. J., Roering C., Hart R. J., Armstrong R. A., de Ronde C., Green R. W. E., Tredoux M., Ellie P. and Hart R. A. (1992) Formation of an Archaean continent. *Nature* **357**, 553–562.

Derry L. A. and Jacobsen S. B. (1990) The chemical evolution of Precambrian seawater: evidence from REEs in banded iron formations. *Geochimica et Cosmochimica Acta* **54**, 2965–2977.

Dessert C., Dupré B., Gaillardet J., François L. M. and Allègre C. J. (2003) Basalt weathering laws and the impact of basalt weathering on the global carbon cycle. *Chemical Geology* **202**, 257–273.

Dhuime B., Hawkesworth C. J., Storey C. D. and Cawood P. A. (2011) From sediments to their source rocks: Hf and Nd isotopes in recent river sediments. *Geology* **39**, 407–410.

Dhuime B., Wuestefeld A. and Hawkesworth C. J. (2015) Emergence of modern continental crust about 3 billion years ago. *Nature Geoscience* **8**, 552–555.

Drabon N., Lowe D. R. and Heubeck C. E. (2014) Petrography of sandstones from drill cores BARB4 and BARB5, Paleoarchean Mapepe Formation, Barberton greenstone belt, South Africa: Implications for provenance and tectonic reconstructions. In Abstract AGU fall meeting. San Francisco.

Eriksson K. A. (1980) Transitional sedimentation styles in the Moodies and Fig Tree Groups, Barberton mountain land, South Africa: evidence favouring an Archean continental margin. *Precambrian Research* **12**, 141–160.

Frost C. D. (1993) Nd isotopic evidence for the antiquity of the Wyoming province. *Geology* **21**, 351–354.

Fryer B. J. (1977) Rare earth evidence in iron-formations for changing Precambrian oxidation states. *Geochimica et Cosmochimica Acta* **41**, 361–367.

Furnes H., de Wit M. and Robins B. (2013) A review of new interpretations of the tectonostratigraphy, geochemistry and evolution of the Onverwacht Suite, Barberton Greenstone Belt, South Africa. *Gondwana Research* **23**, 403–428.

Furnes H., Robins B. and de Wit M. J. (2012) Geochemistry and petrology of lavas in the upper onverwatch suite, Barberton Mountain Land, South Africa. *South African Journal of Geology* **115**, 171–210.

Galic A. (2015) Unravelling atmospheric photolysis and ocean redox chemistry from Paleoarchean pyrite. A multiple sulfur and iron stable isotope study.

Garçon M. and Chauvel C. (2014) Where is basalt in river sediments, and why does it matter?

Earth and Planetary Science Letters **407**, 61–69.

Garçon M., Chauvel C., France-Lanord C., Huyghe P. and Lavé J. (2013) Continental sedimentary processes decouple Nd and Hf isotopes. *Geochimica et Cosmochimica Acta* **121**, 177–195.

Garçon M., Chauvel C., France-Lanord C., Limonta M. and Garzanti E. (2014) Which minerals control the Nd–Hf–Sr–Pb isotopic compositions of river sediments? *Chemical Geology* **364**, 42–55.

Garzanti E., Andò S., France-Lanord C., Censi P., Pietro Vignola, Galy V. and Lupker M. (2011) Mineralogical and chemical variability of fluvial sediments 2. Suspended-load silt (Ganga–Brahmaputra, Bangladesh). *Earth and Planetary Science Letters* **302**, 107–120.

Garzanti E., Andò S., France-Lanord C., Vezzoli G., Censi P., Galy V. and Najman Y. (2010) Mineralogical and chemical variability of fluvial sediments 1. Bedload sand (Ganga–Brahmaputra, Bangladesh). *Earth and Planetary Science Letters* **299**, 368–381.

Gaschnig R. M., Rudnick R. L., McDonough W. F., Kaufman A. J., Hu Z. and Gao S. (2014) Onset of oxidative weathering of continents recorded in the geochemistry of ancient glacial diamictites. *Earth and Planetary Science Letters* **408**, 87–99.

Gaschnig R. M., Rudnick R. L., McDonough W. F., Kaufman A. J., Valley J. W., Hu Z., Gao S. and Beck M. L. (2016) Compositional evolution of the upper continental crust through time, as constrained by ancient glacial diamictites. *Geochimica et Cosmochimica Acta* **186**, 316–343.

Glikson A. Y. (1976) Trace element geochemistry and origin of early Precambrian acid igneous series, Barberton Mountain Land, Transvaal. *Geochimica et Cosmochimica Acta* **40**, 1261–1280.

Griffin W. L., Belousova E. A., O'Neill C., O'Reilly S. Y., Malkovets V., Pearson N. J., Spetsius S. and Wilde S. A. (2014) The world turns over: Hadean–Archean crust–mantle evolution. *Lithos* **189**, 2–15.

Grosch E. G., Kosler J., McLoughlin N., Drost K., Slama J. and Pedersen R. B. (2011) Paleoarchean detrital zircon ages from the earliest tectonic basin in the Barberton Greenstone Belt, Kaapvaal craton, South Africa. *Precambrian Research* **191**, 85–99.

Heubeck C. and Lowe D. R. (1994) Depositional and tectonic setting of the Archean Moodies Group, Barberton Greenstone Belt, South Africa. *Precambrian Research* **68**, 257–290.

Hoffmann J. E., Kröner A., Hegner E., Viehmann S., Xie H., Iaccheri L. M., Schneider K. P., Hofmann A., Wong J., Geng H. and Yang J. (2016) Source composition, fractional crystallization and magma mixing processes in the 3.48–3.43 Ga Tsawela tonalite suite (Ancient Gneiss Complex, Swaziland) – Implications for Palaeoarchaean geodynamics. *Precambrian Research* **276**, 43–66.

Hoffmann J. E., Münker C., Polat A., König S., Mezger K. and Rosing M. T. (2010) Highly depleted Hadean mantle reservoirs in the sources of early Archean arc-like rocks, Isua supracrustal belt, southernWest Greenland. *Geochimica et Cosmochimica Acta* **74**, 7236–7260.

Hofmann A. (2005) The geochemistry of sedimentary rocks from the Fig Tree Group, Barberton greenstone belt: Implications for tectonic, hydrothermal and surface processes during mid-Archaean times. *Precambrian Research* **143**, 23–49.

Hunter D. R. (1970) The ancient gneiss complex in Swaziland. *Transactions of the Geological Society of South Africa* **73**, 107–150.

Hunter D. R., Barker F. and Millard H. T. (1984) Geochemical investigation of Archaean bimodal and Dwalile metamorphic suites, ancient gneiss complex, Swaziland. *Precambrian Research* **24**, 131–155.

Jacobsen S. B. (1988) Isotopic constraints on crustal growth and recycling. *Earth and Planetary Science Letters* **90**, 315–329.

Jacobsen S. B. and Dymek R. F. (1988) Nd and Sr isotope systematics of clastic metasediments from Isua, West Greenland: Identification of pre-3.8 Ga Differentiated Crustal Components. *Journal of Geophysical Research* **93**, 338–354.

Jahn B. M. and Condie K. C. (1995) Evolution of the Kaapvaal Craton as viewed from geochemical and Sm-Nd isotopic analyses of intracratonic pelites. *Geochimica et Cosmochimica Acta* **59**, 2239–2258.

James D. E., Niu F. and Rokosky J. (2003) Crustal structure of the Kaapvaal craton and its significance for early crustal evolution. *Lithos* **71**, 413–429.

Kamber B. S. (2010) Archean mafic–ultramafic volcanic landmasses and their effect on ocean–atmosphere chemistry. *Chemical Geology* **274**, 19–28.

Kamber B. S. and Webb G. E. (2001) The geochemistry of late Archaean microbial carbonate: implications for ocean chemistry and continental erosion history. *Geochimica et Cosmochimica Acta* **65**, 2509–2525.

Kamber B. S., Webb G. E. and Gallagher M. (2014) The rare earth element signal in Archaean microbial carbonate: information on ocean redox and biogenicity. *Journal of the Geological Society* **171**, 745–763.

Kamo S. L. and Davis D. W. (1994) Reassessment of Archean crustal development in the Barberton Mountain Land, South Africa, based on U-Pb dating. *Tectonics* **13**, 167–192.

Keller C. B. and Schoene B. (2012) Statistical geochemistry reveals disruption in secular lithospheric evolution about 2.5 Gyr ago. Nature 485, 490–493.

Kleinhanns I. C., Kramers J. D. and Kamber B. S. (2003) Importance of water for Archaean granitoid petrology: a comparative study of TTG and potassic granitoids from Barberton Mountain Land, South Africa. Contrib Mineral Petrol 145, 377–389.

Kohler E. A. and Anhaeusser C. R. (2002) Geology and geodynamic setting of Archaean silicic metavolcaniclastic rocks of the Bien Venue Formation, Fig Tree Group, northeast Barberton greenstone belt, South Africa. *Precambrian Research* **116**, 199–235.

Kröner A. (2007) Chapter 5.2 The Ancient Gneiss Complex of Swaziland and Environs:

Record of Early Archean Crustal Evolution in Southern Africa. In *Earth's oldest rocks* Developments in Precambrian Geology. Elsevier. pp. 465–480.

Kröner A. and Tegtmeyer A. (1994) Gneiss-greenstone relationships in the Ancient Gneiss Complex of southwestern Swaziland, southern Africa, and implications for early crustal evolution. *Precambrian Research* **67**, 109–139.

Kröner A., Byerly G. R. and Lowe D. R. (1991) Chronology of early Archaean granite-greenstone evolution in the Barberton Mountain Land, South Africa, based on precise dating by single zircon evaporation. *Earth and Planetary Science Letters* **103**, 41–54.

Kröner A., Compston W. and Williams I. S. (1989) Growth of early Archaean crust in the Ancient Gneiss Complex of Swaziland as revealed by single zircon dating. *Tectonophysics* **161**, 271–298.

Kröner A., Hegner E., Wendt J. I. and Byerly G. R. (1996) The oldest part of the Barberton granitoid-greenstone terrain, South Africa: evidence for crust formation between 3.5 and 3.7 Ga. *Precambrian Research* **78**, 105–124.

Kröner A., Hoffmann J. E., Xie H., Munker C. and Hegner E. (2014) Generation of early Archaean grey gneisses through melting of older crust in the eastern Kaapvaal craton, southern Africa. *Precambrian Research* **255**, 823–843.

Kröner A., Hoffmann J. E., Xie H., Wu F., Münker C., Hegner E., Wong J., Wan Y. and Liu D. (2013) Generation of early Archaean felsic greenstone volcanic rocks through crustal melting in the Kaapvaal, craton, southern Africa. *Earth and Planetary Science Letters* **381**, 188–197.

Lahaye Y., Arndt N., Byerly G., Chauvel C., Fourcade S. and Gruau G. (1995) The influence of alteration on the trace-element and Nd isotopic compositions of komatiites. *Chemical Geology* **126**, 43–64.

Ledevin M., Arndt N., Simionovici A., Jaillard E. and Ulrich M. (2014) Silica precipitation triggered by clastic sedimentation in the Archean: New petrographic evidence from cherts of the Kromberg type section, South Africa. *Precambrian Research* **255**, 316–334.

Liu X. M., Kah L. C., Knoll A. H., Cui H., Kaufman A. J., Shahar A. and Hazen R. M. (2015) Tracing Earth's O2 evolution using Zn/Fe ratios in marine carbonates. *Geochem. Persp. Let.* **2**, 24–34.

Lowe D. R. (1994) Accretionary history of the Archean Barberton greenstone belt (3.55-3.22 Ga), southern Africa. *Geology* **22**, 1099–1102.

Lowe D. R. and Byerly G. R. (1999) *Geologic Evolution of the Barberton Greenstone Belt, South Africa*, Geological Society of America - Special Paper 329.

Lowe D. R. and Nocita B. W. (1999) Foreland basin sedimentation in the Mapepe Formation, southern-facies Fig Tree Group. In *Geologic Evolution of the Barberton Greenstone Belt, South Africa* (eds. D. R. Lowe and G. R. Byerly). Geological Society of America Special Papers. pp. 233–258.

Lupker M., France-Lanord C., Lavé J., Bouchez J., Galy V., Métivier F., Gaillardet J.,

Lartiges B. and Mugnier J.-L. (2011) A Rouse-based method to integrate the chemical composition of river sediments: Application to the Ganga basin. *Journal of Geophysical Research* **116**, F04012.

McLennan S. M. (1989) Rare earth elements in sedimentary rocks: influence of provenance and sedimentary processes. In *Geochemistry and mineralogy of rare earth elements* (eds. B. R. Lipin and G. A. McKay). Reviews in Mineralogy and Geochemistry. pp. 169–200.

Moyen J.-F., Stevens G. and Kisters A. (2006) Record of mid-Archaean subduction from metamorphism in the Barberton terrain, South Africa. *Nature* **442**, 559–562.

Nair S. K., Gao S. S., Liu K. H. and Silver P. G. (2006) Southern African crustal evolution and composition: Constraints from receiver function studies. *Journal of Geophysical Research* **111**, 1–17.

Nance W. B. and Taylor S. R. (1976) Rare earth element patterns and crustal evolution-1. Australian post-Archean sedimentary rocks. *Geochimica et Cosmochimica Acta* **40**, 1539–1551.

Nocita B. W. (1989) Sandstone petrology of the Archean Fig Tree Group, Barberton greenstone belt, South Africa: Tectonic implications. *Geology* **17**, 953–956.

Paris I., Stanistreet I. G. and Hughes M. J. (1985) Cherts of the Barberton greenstone belt interpreted as products of submarine exhalative activity. *The Journal of Geology* **93**, 111–129.

Patchett P. J., White W. M., Feldmann H., Kielinczuk S. and Hofmann A. W. (1984) Hafnium/rare earth element fractionation in the sedimentary system and crustal recycling into the Earth's mantle. *Earth and Planetary Science Letters* **69**, 365–378.

Puchtel I. S., Blichert-Toft J., Touboul M., Walker R. J., Byerly G. R., Nisbet E. G. and Anhaeusser C. R. (2013) Insights into early Earth from Barberton komatiites: Evidence from lithophile isotope and trace element systematics. *Geochimica et Cosmochimica Acta* **108**, 63–90.

Robin-Popieul C. C. M., Arndt N. T., Chauvel C., Byerly G. R., Sobolev A. V. and Wilson A. (2012) A New Model for Barberton Komatiites: Deep Critical Melting with High Melt Retention. *Journal of Petrology* **53**, 2191–2229.

Rouchon V. and Orberger B. (2008) Origin and mechanisms of K–Si-metasomatism of ca. 3.4–3.3Ga volcaniclastic deposits and implications for Archean seawater evolution: Examples from cherts of Kittys Gap (Pilbara craton, Australia) and Msauli (Barberton Greenstone Belt, South Africa). *Precambrian Research* **165**, 169–189.

Rudnick R. L. and Fountain D. M. (1995) Nature and composition of the continental crust: A lower crustal perspective. *Reviews of Geophysics* **33**, 267–309.

Rudnick R. L. and Gao S. (2014) 4.1 - Composition of the Continental Crust. In *Treatise on Geochemistry (Second Edition)* (ed. H. D. H. K. Turekian). Treatise on Geochemistry (Second Edition). Elsevier, Oxford. pp. 1–51.

Sauzéat L., Rudnick R. L., Chauvel C., Garçon M. and Tang M. (2015) New perspectives on

1095 the Li isotopic composition of the upper continental crust and its weathering signature.
1096 *Earth and Planetary Science Letters* **428**, 181–192.

1097 Schoene B. and Bowring S. A. (2010) Rates and mechanisms of Mesoarchean magmatic arc
1098 construction, eastern Kaapvaal craton, Swaziland. *Geological Society of America Bulletin*
1099 **122**, 408–429.

1100 Schoene B., de Wit M. J. and Bowring S. A. (2008) Mesoarchean assembly and stabilization
1101 of the eastern Kaapvaal craton: A structural-thermochronological perspective. *Tectonics*
1102 **27**, 1–27.

1103 Schoene B., Dudas F. O. L., Bowring S. A. and de Wit M. (2009) Sm-Nd isotopic mapping of
1104 lithospheric growth and stabilization in the eastern Kaapvaal craton. *Terra Nova* **21**, 219–
1105 228.

1106 Stiegler M. T., Cooper M., Byerly G. R. and Lowe D. R. (2012) Geochemistry and petrology
1107 of komatiites of the Pioneer Ultramafic Complex of the 3.3 Ga Weltevreden Formation,
1108 Barberton greenstone belt, South Africa. *Precambrian Research* **212-213**, 1–12.

1109 Tang M., Chen K. and Rudnick R. L. (2016) Archean upper crust transition from mafic to
1110 felsic marks the onset of plate tectonics. *Science* **351**, 372–375.

1111 Taylor S. R. and McLennan S. M. (1985) *The continental crust: Its composition and*
1112 *evolution*, Blackwell Scientific Pub.,Palo Alto, CA.

1113 Thompson D. A., Bastow I. D., Helffrich G., Kendall J.-M., Wookey J., Snyder D. B. and
1114 Eaton D. W. (2010) Precambrian crustal evolution: Seismic constraints from the
1115 Canadian Shield. *Earth and Planetary Science Letters* **297**, 655–666.

1116 Thurston P. C., Kamber B. S. and Whitehouse M. (2012) Archean cherts in banded iron
1117 formation: Insight into Neoarchean ocean chemistry and depositional processes.
1118 *Precambrian Research* **214-215**, 227–257.

1119 Tice M. M. and Lowe D. R. (2006) The origin of carbonaceous matter in pre-3.0 Ga
1120 greenstone terrains: A review and new evidence from the 3.42 Ga Buck Reef Chert. *Earth*
1121 *Science Reviews* **76**, 259–300.

1122 Toulkeridis T., Clauer N., Kröner A., Reimer T. and Todt W. (1999) Characterization,
1123 provenance, and tectonic setting of Fig Tree greywackes from the Archaean Barberton
1124 greenstone belt, South Africa. *Sedimentary Geology* **124**, 113–129.

1125 Toulkeridis T., Goldstein S. L., Clauer N. and Kröner A. (1994) Sm-Nd dating of Fig Tree
1126 clay minerals of the Barberton greenstone belt, South Africa. *Geology* **22**, 199–202.

1127 Toulkeridis T., Goldstein S. L., Clauer N. and Kröner A. (1998) Sm–Nd, Rb–Sr and Pb–Pb
1128 dating of silicic carbonates from the early Archaean Barberton Greenstone Belt, South
1129 Africa: evidence for post-depositional isotopic resetting at low temperature. *Precambrian*
1130 *Research* **92**, 129–144.

1131 Van Kranendonk M. J., Kröner A., Hegner E. and Connelly J. (2009) Age, lithology and
1132 structural evolution of the c. 3.53 Ga Theespruit Formation in the Tjakastad area,
1133 southwestern Barberton Greenstone Belt, South Africa, with implications for Archaean

tectonics. *Chemical Geology* **261**, 115–139.

Vervoort J. D., Patchett P. J. and Blichert-Toft J. (1999) Relationships between Lu–Hf and Sm–Nd isotopic systems in the global sedimentary system. *Earth and Planetary Science Letters* **168**, 79–99.

Viehmann S., Hoffmann J. E., Munker C. and Bau M. (2014) Decoupled Hf-Nd isotopes in Neoarchean seawater reveal weathering of emerged continents. *Geology* **42**, 115–118.

Viljoen M. J. and Viljoen R. P. (1969) An introduction to the geology of the Barberton, granite-greenstone terrain. *Geological Society of South Africa, Special Publication* **2**, 9–28.

Weis D. and Wasserburg G. J. (1987) Rb-Sr and Sm-Nd Systematics of Cherts and Other Siliceous Deposits. *Geochimica et Cosmochimica Acta* **51**, 959–972.

Yamashita K. and Creaser R. A. (1999) Geochemical and Nd isotopic constraints for the origin of Late Archean turbidites from the Yellowknife area, Northwest Territories, Canada. *Geochimica et Cosmochimica Acta* **63**, 2579–2598.

Yamashita K., Creaser R. A. and Villeneuve M. E. (2000) Integrated Nd isotopic and U–Pb detrital zircon systematics of clastic sedimentary rocks from the Slave Province, Canada: evidence for extensive crustal reworking in the early- to mid-Archean. *Earth and Planetary Science Letters* **174**, 283–299.

Youssof M., Thybo H., Artemieva I. M. and Levander A. (2013) Moho depth and crustal composition in Southern Africa. *Tectonophysics* **609**, 267–287.

Zeh A., Gerdes A. and Barton J. M. (2009) Archean Accretion and Crustal Evolution of the Kalahari Craton--the Zircon Age and Hf Isotope Record of Granitic Rocks from Barberton/Swaziland to the Francistown Arc. *Journal of Petrology* **50**, 933–966.

Zeh A., Gerdes A. and Heubeck C. (2013) U-Pb and Hf isotope data of detrital zircons from the Barberton Greenstone Belt: constraints on provenance and Archaean crustal evolution. *Journal of the Geological Society* **170**, 215–223.

Zeh A., Gerdes A. and Millonig L. (2011) Hafnium isotope record of the Ancient Gneiss Complex, Swaziland, southern Africa: evidence for Archaean crust-mantle formation and crust reworking between 3.66 and 2.73 Ga. *Journal of the Geological Society* **168**, 953–964.

Table 1

Table 1: Sm-Nd and Lu-Hf isotopic compositions of metasedimentary rocks from the Barberton area and meta-igneous rocks from the Ancient Gneiss Complex.

Sample name	Depth (m)	Unit/Formation	Type of sample	PCA result	Sm (ppm)	Nd (ppm)	$^{147}Sm/^{144}Nd$	$^{143}Nd/^{144}Nd_0$	$2s_N$	$^{143}Nd/^{144}Nd$ at 3.23Ga	ε_{Nd} at 3.23Ga	Lu (ppm)	Hf (ppm)
Metasedimentary rocks from BARB 4 drill core													
BARB4-119.17	119.17	Fig Tree/Mapepe Fm	Very coarse- grained sandstone	Si-rich	0.62	2.80	0.1338	0.511202	0.000006	0.508345	-2.0	0.076	1.038
BARB4-122.31	122.31	Fig Tree/Mapepe Fm	Fine-grained sandstone	Ca-, Fe- rich	1.39	5.38	0.1565	0.511728	0.000005	0.508386	-1.2	0.133	0.798
BARB4-123.50	123.5	Fig Tree/Mapepe Fm	Mudstone	Crustal detritus- rich	2.87	12.68	0.1368	0.511311	0.000005	0.508390	-1.1	0.299	2.408
BARB4-129.19	129.19	Fig Tree/Mapepe Fm	Fine-grained sandstone	Si-rich	1.03	4.37	0.1425	0.511453	0.000008	0.508411	-0.7	0.143	1.654
BARB4-133.61	133.61	Fig Tree/Mapepe Fm	Coarse-grained sandstone	Si-rich	1.11	4.46	0.1507	0.511659	0.000011	0.508442	-0.1	0.131	1.362
BARB4-134.67	134.67	Fig Tree/Mapepe Fm	Mudstone	Ca-, Fe- rich	1.61	7.04	0.1380	0.511435	0.000003	0.508489	0.8	0.163	0.902
BARB4-141.64	141.64	Fig Tree/Mapepe Fm	Fine-grained sandstone	Ca-, Fe- rich	1.40	5.72	0.1474	0.511571	0.000004	0.508424	-0.4	0.131	0.995
BARB4-145.67	145.67	Fig Tree/Mapepe Fm	Very coarse- grained sandstone	Si-rich	0.74	3.31	0.1343	0.511232	0.000005	0.508364	-1.6	0.080	1.380
Duplicate					*0.72*	*3.23*	*0.1348*	*0.511228*	*0.000004*	*0.508351*	*-1.9*	*0.079*	*1.339*
BARB4-155.69	155.69	Fig Tree/Mapepe Fm	Coarse-grained sandstone	Si-rich	0.99	4.20	0.1423	0.511427	0.000007	0.508388	-1.1	0.110	1.218
Duplicate					*1.03*	*4.35*	*0.1428*	*0.511444*	*0.000004*	*0.508395*	*-1.0*	*0.112*	*1.327*
BARB4-197.64	197.64	Fig Tree/Mapepe Fm	Coarse-grained sandstone	Si-rich	0.82	3.58	0.1382	0.511373	0.000010	0.508423	-0.5	0.080	1.387
BARB4-208.90	208.9	Fig Tree/Mapepe Fm	Coarse-grained sandstone	Si-rich	1.14	5.04	0.1363	0.511329	0.000006	0.508419	-0.5	0.144	1.547
BARB4-314.33	314.33	Fig Tree/Mapepe Fm	Very coarse-grained sandstone	Si-rich	1.02	4.71	0.1311	0.511155	0.000007	0.508355	-1.8	0.133	1.246
BARB4-338.47	338.47	Fig Tree/Mapepe Fm	Mudstone	Crustal detritus- rich	3.35	15.39	0.1316	0.511196	0.000005	0.508387	-1.2	0.300	2.905
BARB4-346.46	346.46	Fig Tree/Mapepe Fm	Mudstone	Crustal detritus- rich	3.90	18.78	0.1255	0.511116	0.000006	0.508437	-0.2	0.409	3.131
Duplicate					*3.89*	*18.95*	*0.1241*	*0.511117*	*0.000004*	*0.508468*	*0.4*	*0.411*	*3.147*
Metasedimentary rocks from BARB 5 drill core													
BARB5-102.68	102.68	Fig Tree/Mapepe Fm	Mudstone	Ca-, Fe- rich	1.49	7.39	0.1217	0.511132	0.000004	0.508534	1.7	0.204	0.662
BARB5-108.46	108.46	Fig Tree/Mapepe Fm	Fine-grained sandstone	Crustal detritus- rich	6.18	31.87	0.1173	0.510917	0.000011	0.508412	-0.7	0.385	8.694
BARB5-315.46	315.46	Fig Tree/Mapepe Fm	Mudstone	Crustal detritus- rich	2.04	9.63	0.1278	0.511143	0.000004	0.508414	-0.6	0.206	2.102
BARB5-319.79	319.79	Fig Tree/Mapepe Fm	Fine-grained sandstone	Crustal detritus- rich	3.05	15.24	0.1208	0.510946	0.000004	0.508367	-1.6	0.265	3.383
Duplicate						*13.69*		*0.510961*	*0.000006*			*0.246*	*3.280*
BARB5-349.44	349.44	Fig Tree/Mapepe Fm	Coarse-grained sandstone	Si-rich	1.18	5.45	0.1311	0.511169	0.000004	0.508371	-1.5	0.127	1.442
BARB5-355.54	355.54	Fig Tree/Mapepe Fm	Coarse-grained sandstone	Ca-, Fe- rich	0.55	2.37	0.1392	0.511384	0.000004	0.508412	-0.7	0.060	0.329
Duplicate					*0.55*	*2.39*	*0.1391*	*0.511356*	*0.000003*	*0.508387*	*-1.2*	*0.056*	*0.313*
BARB5-425.78	425.78	Fig Tree/Mapepe Fm	Mudstone	Ca-, Fe- rich	1.80	9.72	0.1117	0.510909	0.000004	0.508524	1.5	0.172	1.891
BARB5-429.38	429.38	Fig Tree/Mapepe Fm	Mudstone	Ca-, Fe- rich	1.41	6.49	0.1313	0.511157	0.000004	0.508354	-1.8	0.151	1.732
BARB5-520.31	520.31	Fig Tree/Mapepe Fm	Mudstone	Crustal detritus- rich	2.62	12.34	0.1282	0.511125	0.000004	0.508388	-1.1	0.213	2.552
BARB5-615.03	615.03	Fig Tree/Mapepe Fm	Mudstone	Crustal detritus- rich	2.52	11.52	0.1325	0.511226	0.000005	0.508397	-1.0	0.220	2.205
BARB5-620.45	620.45	Fig Tree/Mapepe Fm	Mudstone	Crustal detritus- rich	2.53	11.51	0.1330	0.511215	0.000004	0.508375	-1.4	0.252	2.524
BARB5-724.69	724.69	Fig Tree/Mapepe Fm	Mudstone	Crustal detritus- rich	2.07	9.62	0.1303	0.511155	0.000002	0.508373	-1.4	0.212	1.865
BARB5-730.51	730.51	Fig Tree/Mapepe Fm	Mudstone	Crustal detritus- rich	2.78	12.92	0.1300	0.511226	0.000005	0.508451	0.1	0.298	2.317
Chert samples from BARB 3 drilled in Buck Reef													
B3-227-Ch1	227.34	Buck Reef	Black chert		0.12	0.50	0.1437	0.511465	0.000003	0.508397	-1.0	0.030	0.023
B3-227-Ch2	227.34	Buck Reef	Translucent chert		0.01	0.03	0.2893	0.514615	0.000006	0.508440	-0.1	0.006	0.007
B3-402-Ch3	402.9	Buck Reef	Chert breccia		2.16	7.25	0.1796	0.512258	0.000003	0.508423	-0.4	0.406	0.042
Meta-igneous rocks from the Ancient Gneiss Complex													
KV84-2A		Dwalile suite	Amphibolite		0.29	1.19	0.1464	0.511466	0.000005	0.508340	-2.1	0.025	0.475
Duplicate					*0.29*	*1.26*	*0.1405*	*0.511351*	*0.000015*	*0.508351*	*-1.7*		
KV84-2B		Dwalile suite	Amphibolite		2.59	9.55	0.1639	0.511890	0.000006	0.508391	-1.1		
KV84-2C		Dwalile suite	Amphibolite		3.60	13.77	0.1582	0.511708	0.000014	0.508330	-2.3		
KV84-5B		Dwalile suite	Amphibolite		1.00	3.23	0.1873	0.512410	0.000017	0.508411	-0.7		
SWZ-12		Dwalile suite	Metabasalt		0.77	2.25	0.2078	0.512946	0.000029	0.508509	1.2		
KV84-5C		Ngwane	Garnet amphibolite		8.69	37.33	0.1407	0.511386	0.000034	0.508381	-1.3		
KV84-5D		Ngwane	Garnet amphibolite		4.63	25.29	0.1107	0.510713	0.000004	0.508349	-1.9	0.311	3.036
Duplicate					*4.49*	*24.58*	*0.1105*	*0.510668*	*0.000018*	*0.508309*	*-2.5*		
KV84-1A		Ngwane	Grey gneiss		5.10	27.63	0.1115	0.510703	0.000028	0.508323	-2.4		
SWZ-4		Ngwane	Quartz monzonite gneiss		2.39	16.09	0.0898	0.510293	0.000018	0.508376	-1.4		
SWZ-5		Ngwane	Siliceous gneiss		9.66	45.53	0.1282	0.511086	0.000020	0.508350	-1.9		
SWZ-10		Ngwane	Metabasalt		1.68	5.21	0.1953	0.512668	0.000029	0.508498	1.0		
SWZ-19		Ngwane	Amphibolite		3.69	18.42	0.1210	0.510882	0.000004	0.508299	-2.9	0.271	2.133
Duplicate					*3.68*	*18.59*	*0.1197*	*0.510913*	*0.000025*	0.508358	*-1.7*		
SWZ 29		Ngwane	Amphibolite		3.08	10.41	0.1789	0.512308	0.000038	0.508488	*0.8*		
SW-31		Ngwane	Siliceous gneiss		18.18	71.07	0.1547	0.511721	0.000003	0.508419	-0.5	2.692	14.142
Duplicate					*18.06*	*71.12*	*0.1536*	*0.511687*	*0.000003*	*0.508408*	*-0.7*	*2.625*	*14.490*

Figure 1

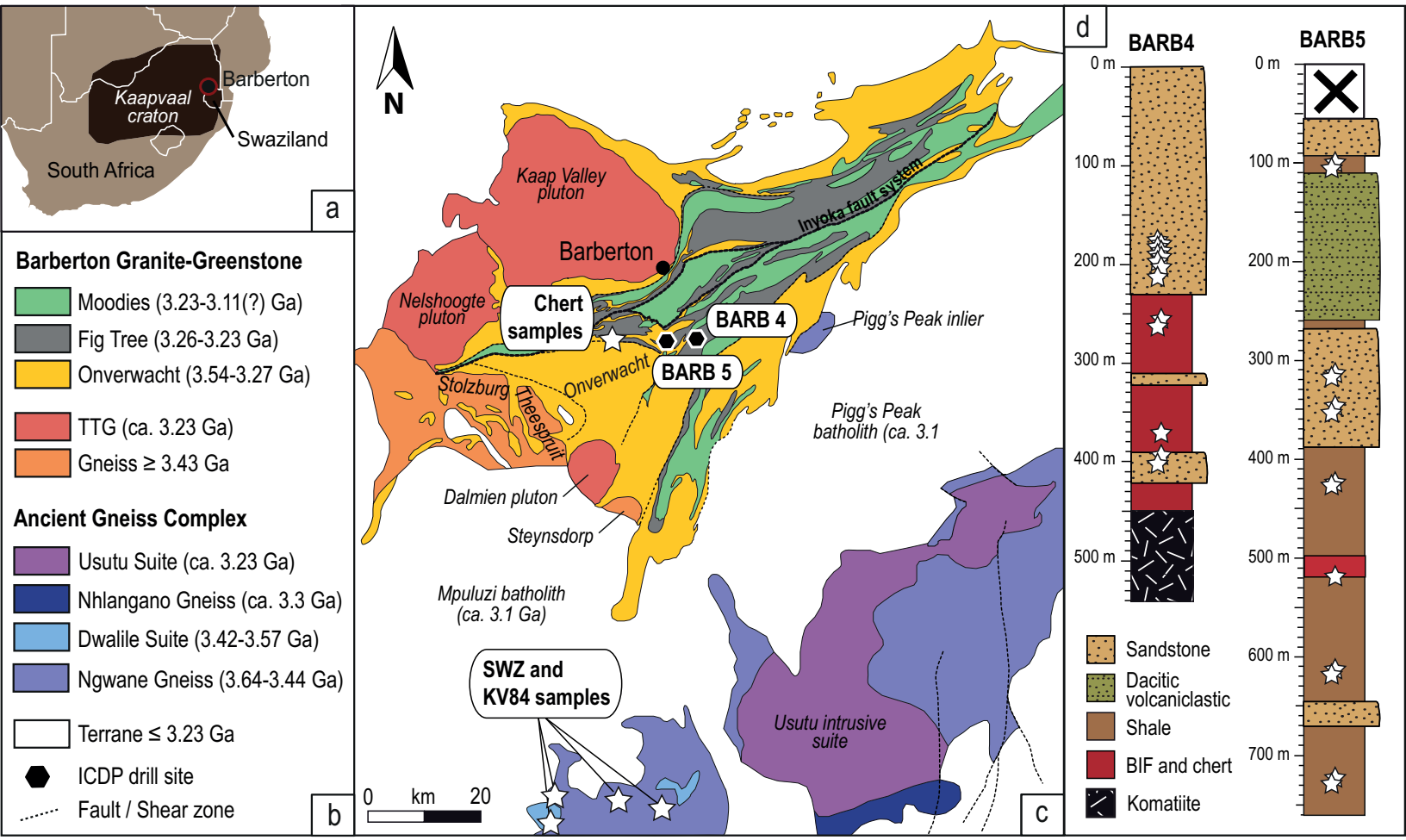

Figure 1

Figure 2

Figure 2

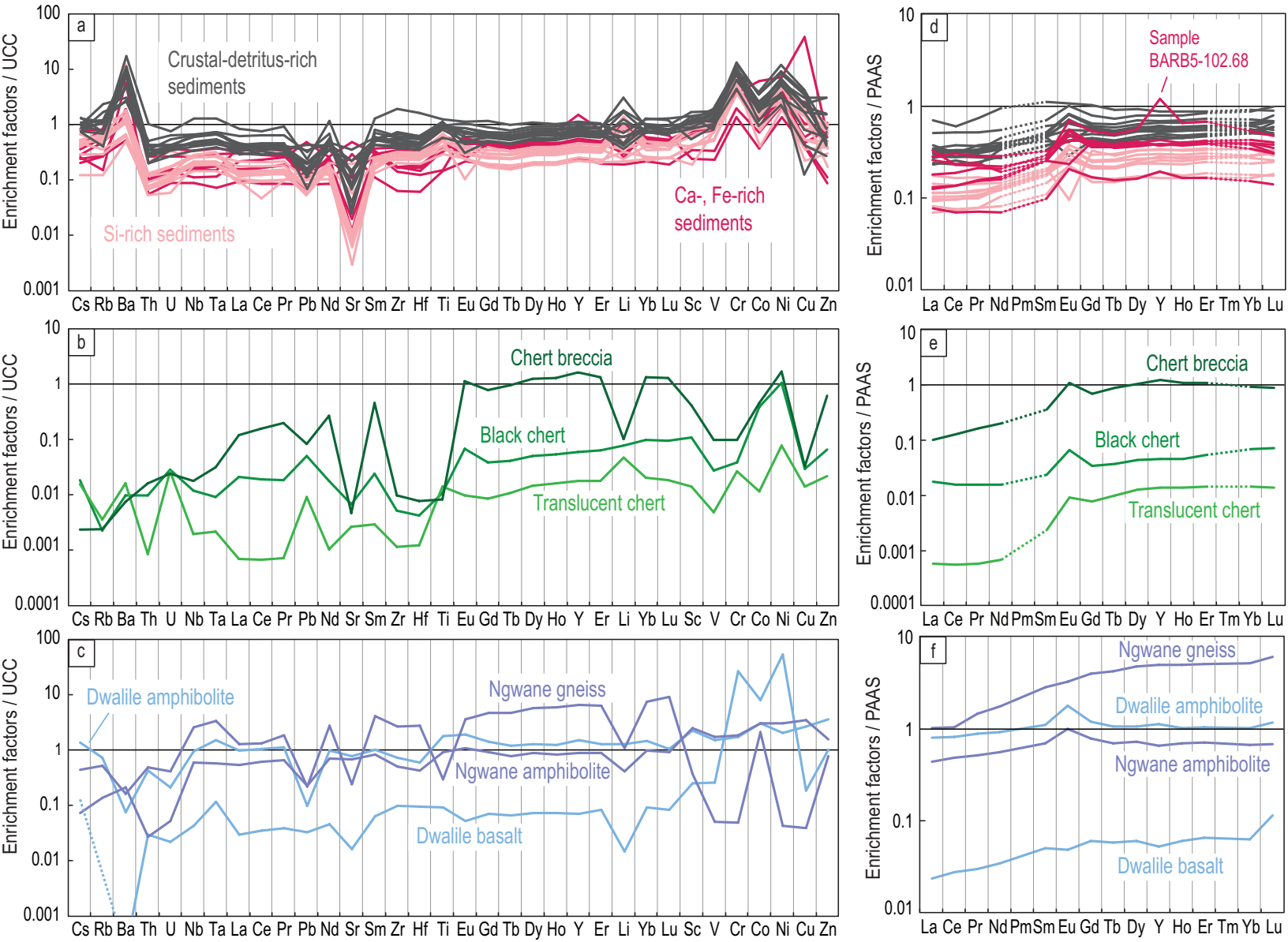

Figure 3

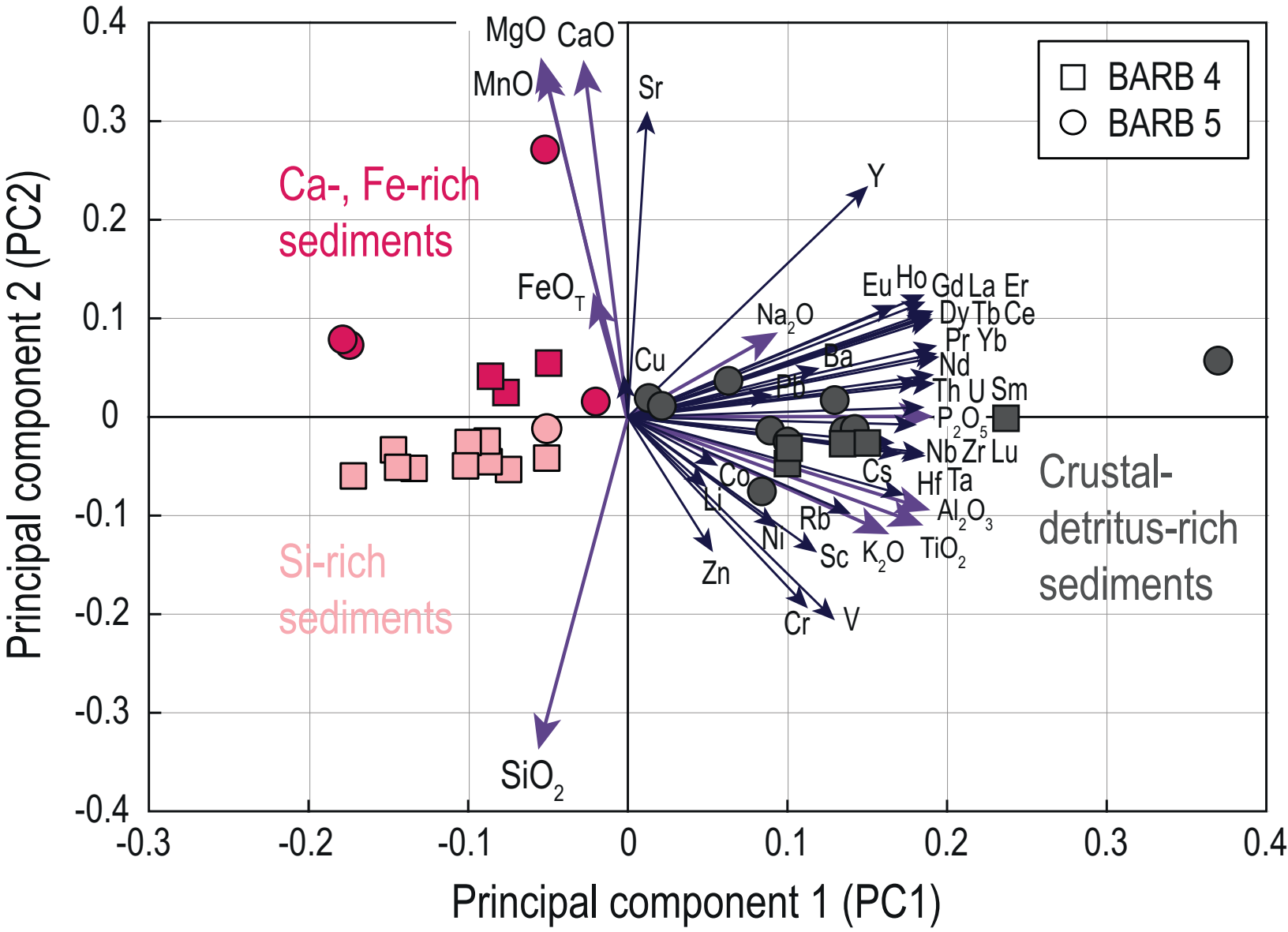
BARB 4
BARB 5
Ca-, Fe-rich sediments
Si-rich sediments
Crustal-detritus-rich sediments
MgO
CaO
MnO
Sr
Y
FeO$_T$
Na$_2$O
Cu
Ba
Pb
Eu Ho Gd La Er
Dy Tb Ce
Pr Yb
Nd
Th U Sm
P$_2$O$_5$
Nb Zr Lu
Cs
Hf Ta
Al$_2$O$_3$
TiO$_2$
K$_2$O
Sc
Rb
Ni
Co
Li
Zn
Cr
V
SiO$_2$
0.4
0.3
0.2
0.1
0
-0.1
-0.2
-0.3
-0.4
-0.3
-0.2
-0.1
0
0.1
0.2
0.3
0.4
Principal component 2 (PC2)
Principal component 1 (PC1)

Figure 4

Figure 4

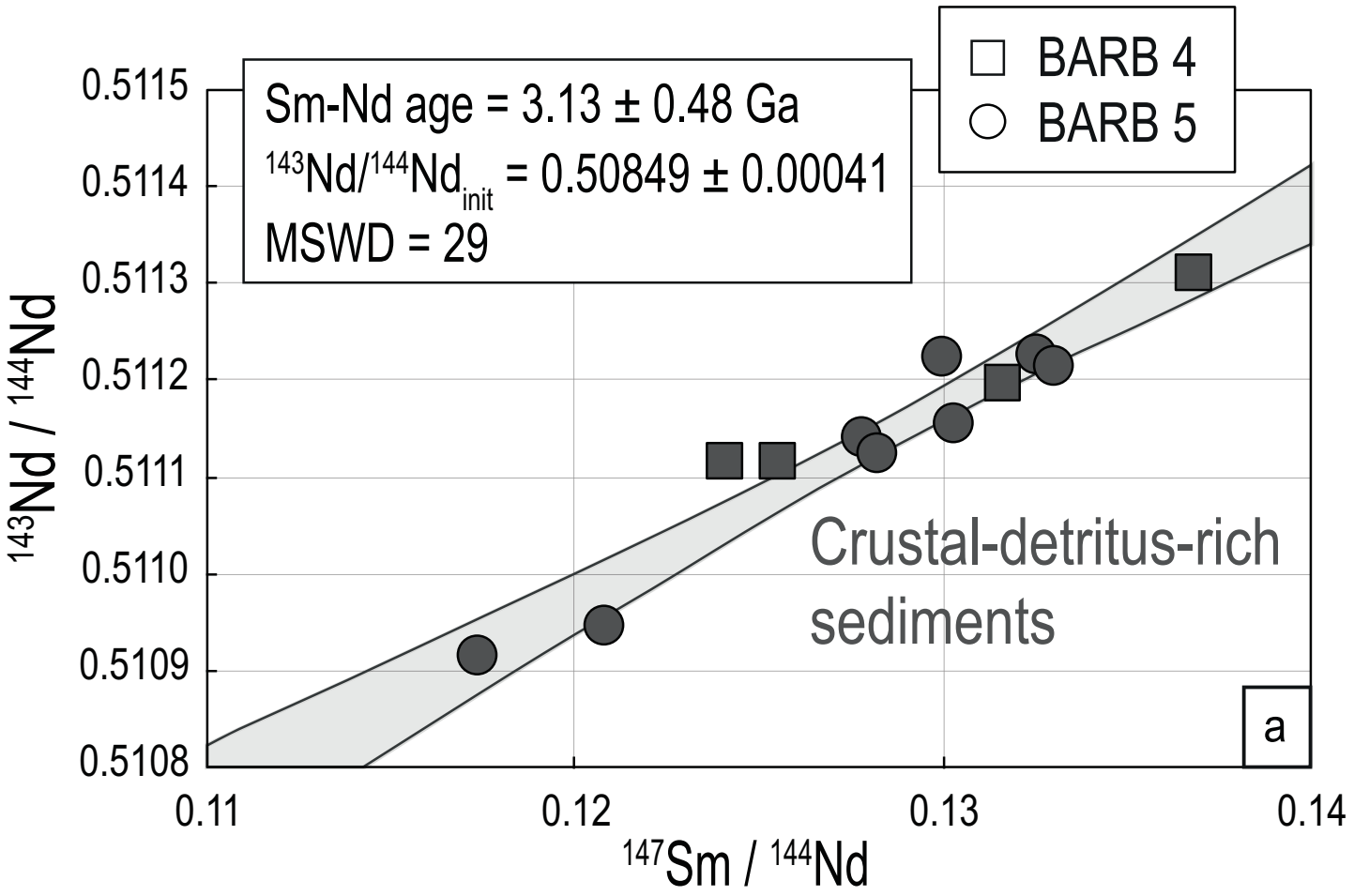

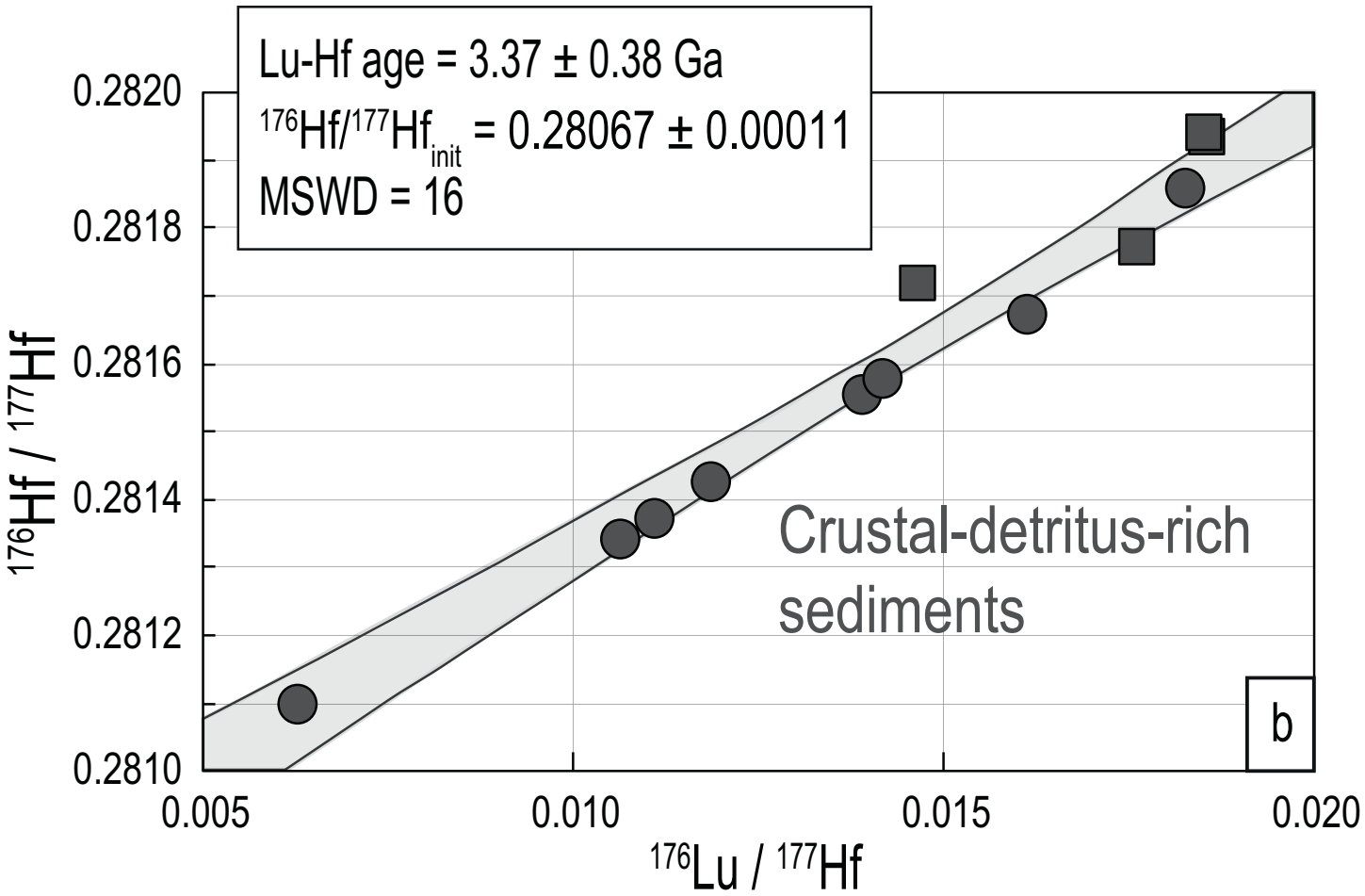

Figure 5

Figure 5

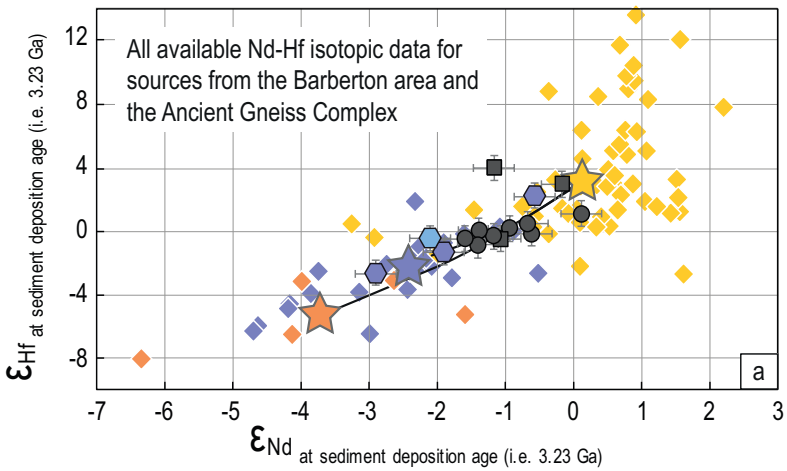

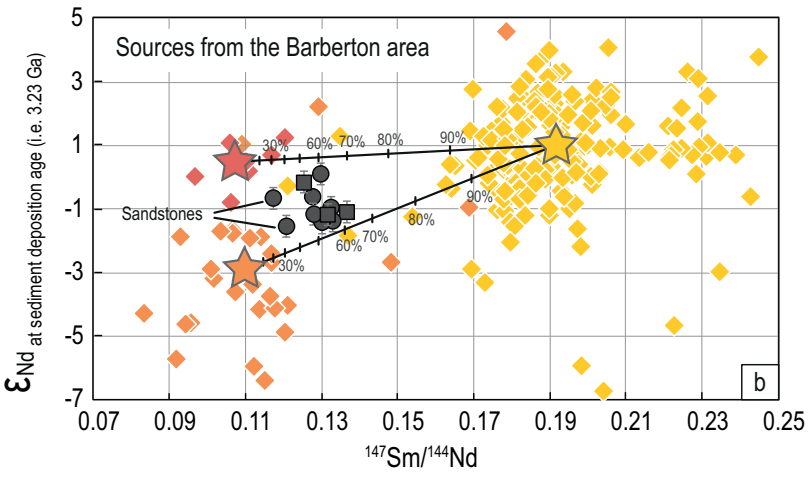

This study

Barberton Greenstone Belt

Crustal detritus-rich sediments

- BARB 4 - Fig Tree group
- BARB 5 - Fig Tree group

Ancient Gneiss Complex

- Ngwane unit
- Dwalile suite

Literature data

Barberton Greenstone Belt

- Young felsic rocks (3.23-3.26 Ga)
- Old felsic rocks (3.45-3.53 Ga)
- Mafic and ultra-mafic rocks (3.27-3.53 Ga)

Ancient Gneiss Complex

- Young felsic rocks (3.23-3.33 Ga)
- Old felsic rocks (>3.45 Ga)
- Mafic and ultra-mafic rocks (>3.45 Ga)

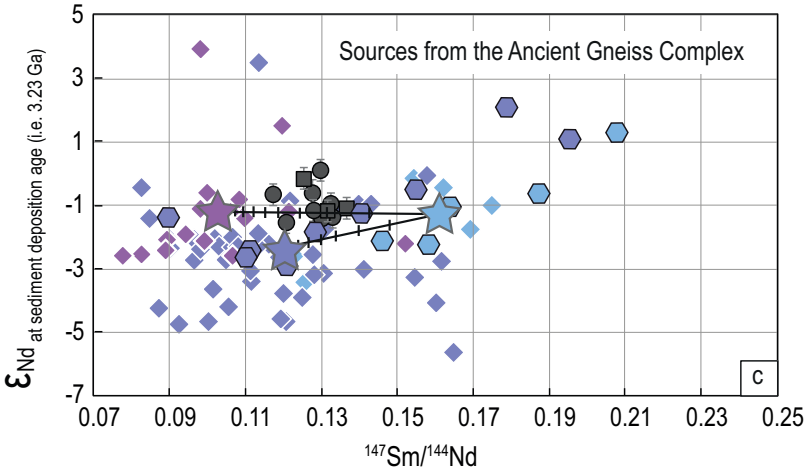

Figure 6

Figure 6

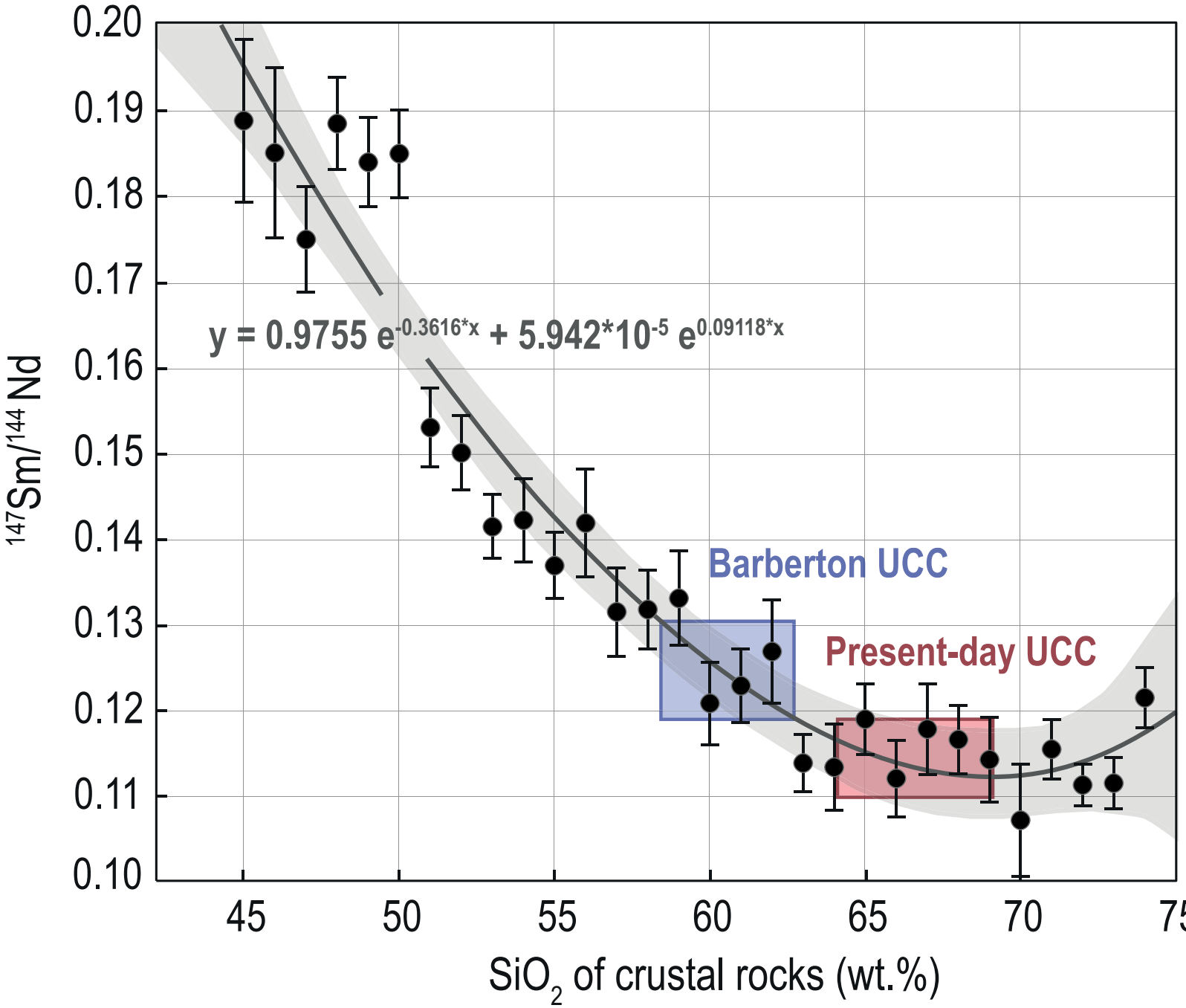

Figure 7

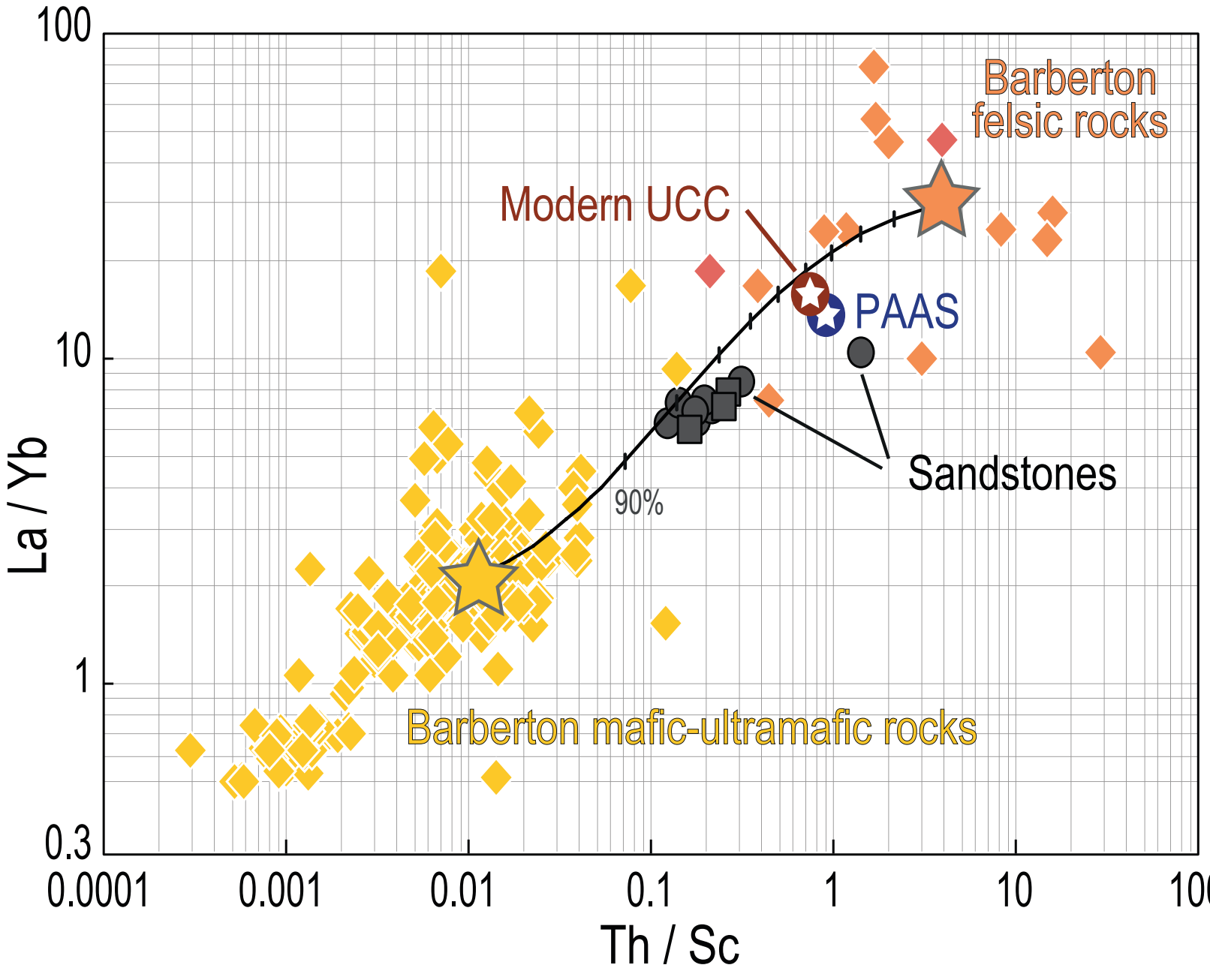
100
10
1
0.3
La / Yb
0.0001
0.001
0.01
0.1
1
10
100
Th / Sc
Barberton
felsic rocks
Modern UCC
PAAS
Sandstones
90%
Barberton mafic-ultramafic rocks

Figure 8

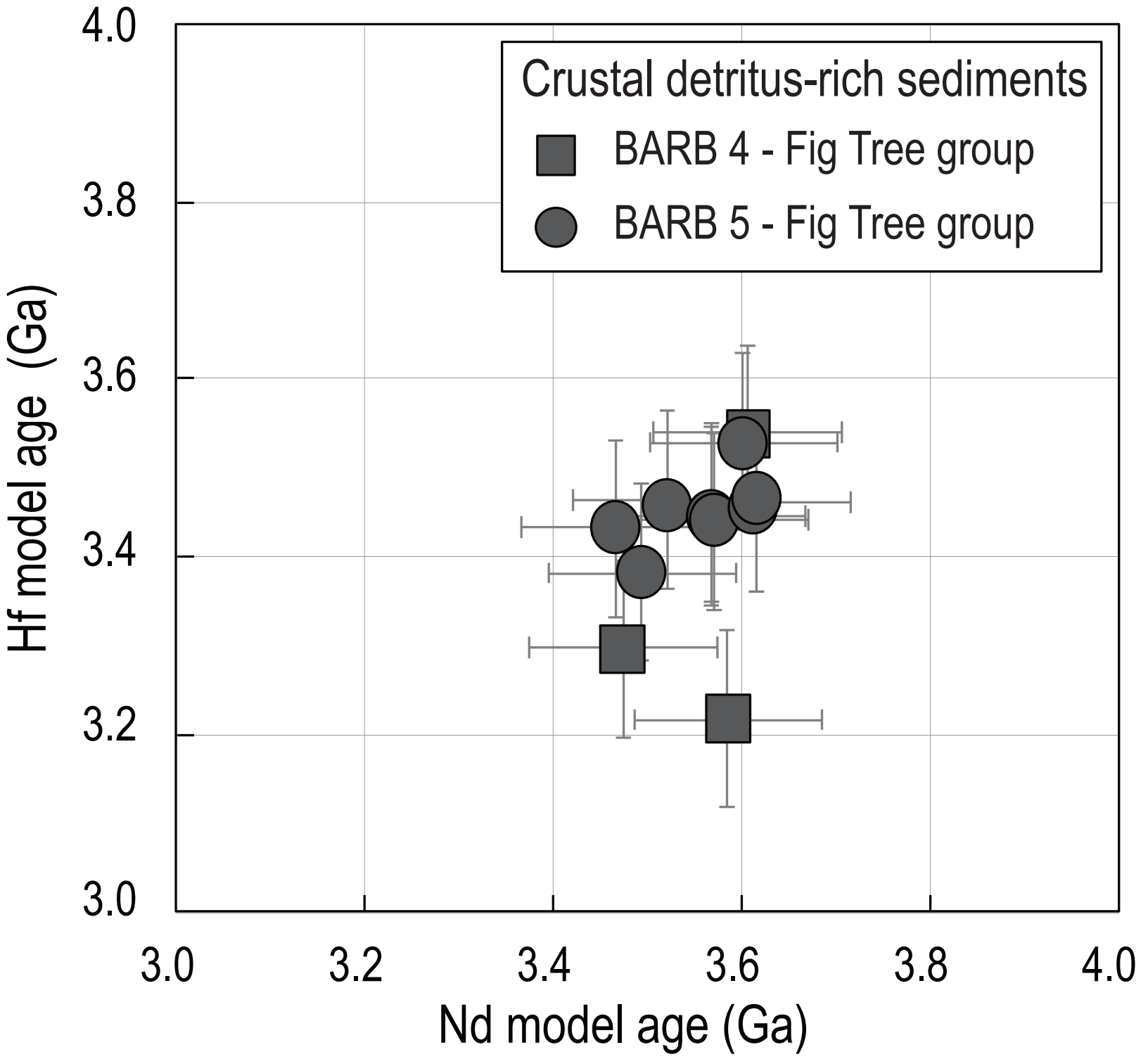
Crustal detritus-rich sediments
BARB 4 - Fig Tree group
BARB 5 - Fig Tree group
Hf model age (Ga)
Nd model age (Ga)
4.0
3.8
3.6
3.4
3.2
3.0
3.0
3.2
3.4
3.6
3.8
4.0

Figure 9

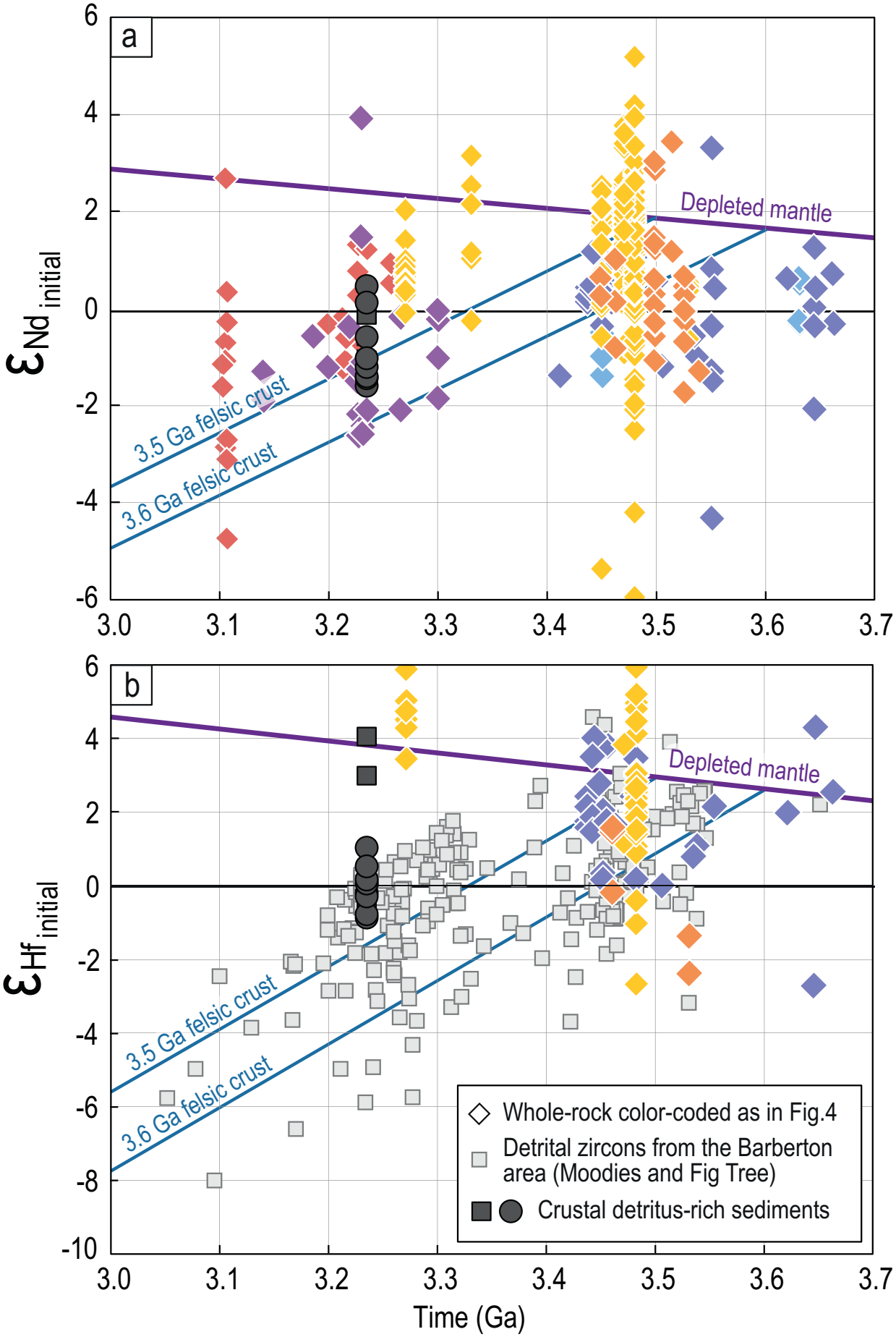
a
b
Depleted mantle
3.5 Ga felsic crust
3.6 Ga felsic crust
εNd initial
εHf initial
Time (Ga)
Whole-rock color-coded as in Fig.4
Detrital zircons from the Barberton area (Moodies and Fig Tree)
Crustal detritus-rich sediments

Figure 10

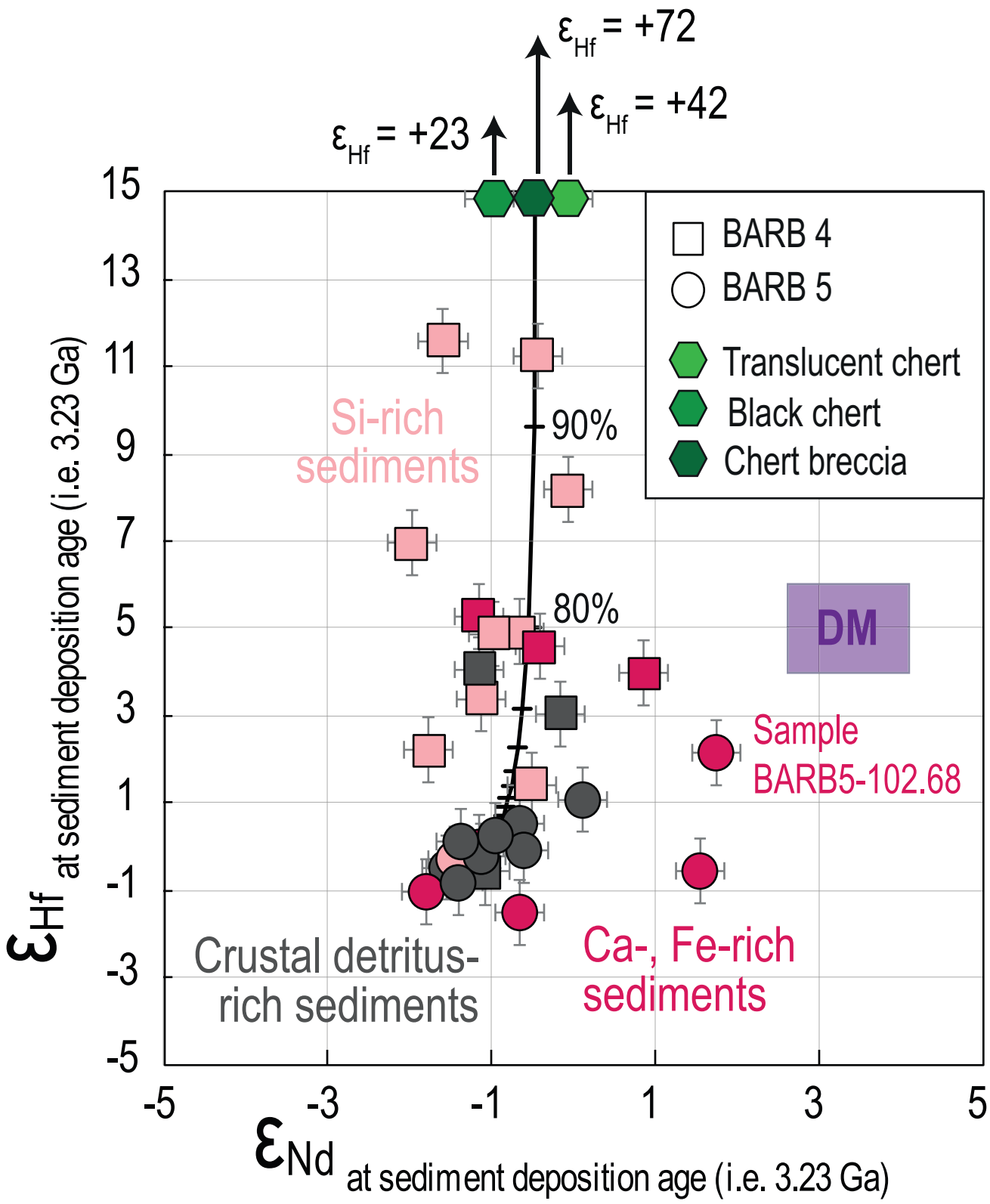
ε_{Hf} = +72
ε_{Hf} = +42
ε_{Hf} = +23
BARB 4
BARB 5
Translucent chert
Black chert
Chert breccia
Si-rich sediments
90%
80%
DM
Sample BARB5-102.68
Crustal detritus-rich sediments
Ca-, Fe-rich sediments
ε_{Hf} at sediment deposition age (i.e. 3.23 Ga)
ε_{Nd} at sediment deposition age (i.e. 3.23 Ga)
15
13
11
9
7
5
3
1
-1
-3
-5
-5
-3
-1
1
3
5

Figure 11

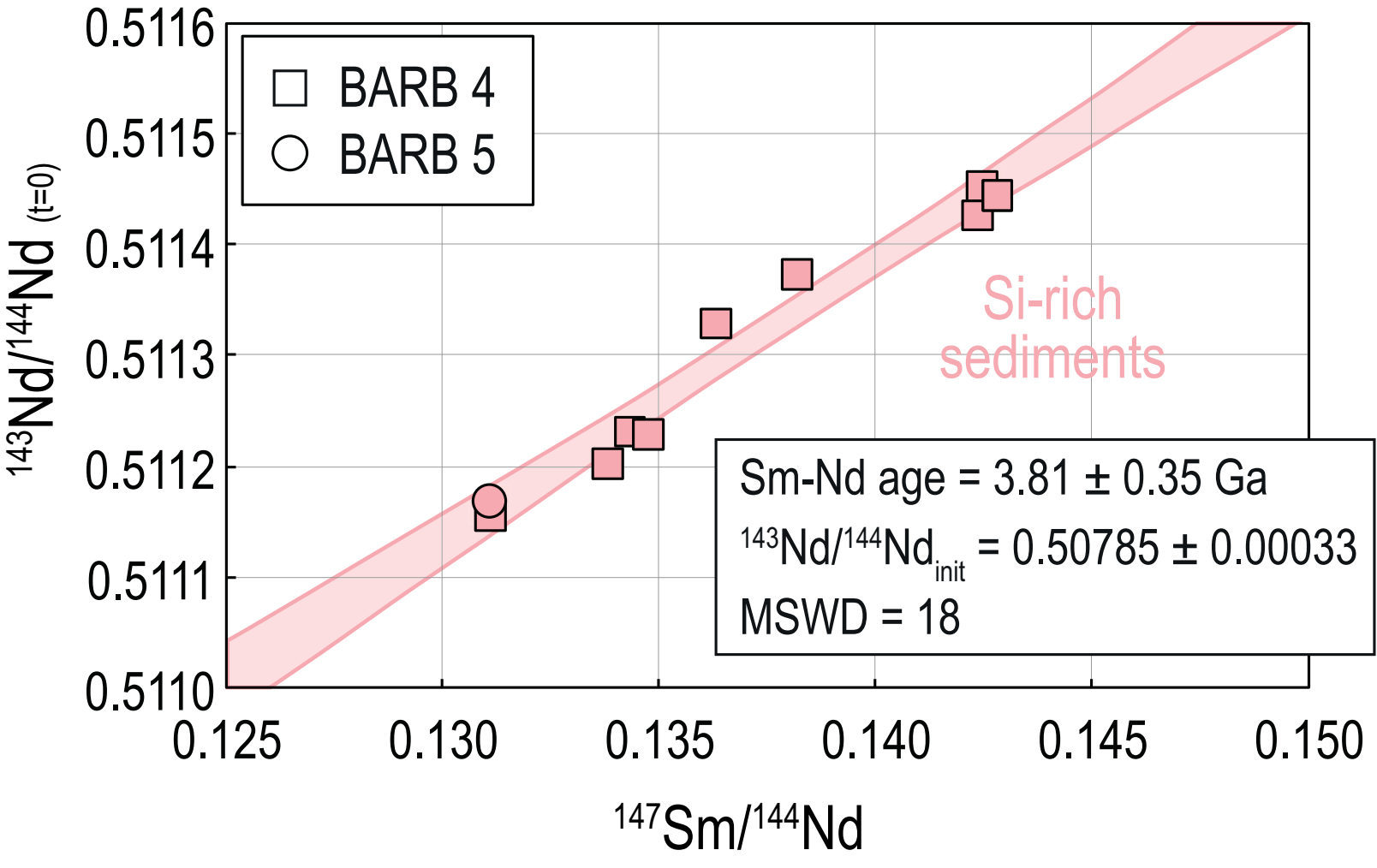
BARB 4
BARB 5
Si-rich sediments
Sm-Nd age = 3.81 ± 0.35 Ga
143Nd/144Nd init = 0.50785 ± 0.00033
MSWD = 18
143Nd/144Nd (t=0)
147Sm/144Nd
0.5116
0.5115
0.5114
0.5113
0.5112
0.5111
0.5110
0.125
0.130
0.135
0.140
0.145
0.150

Figure 12

Figure 12

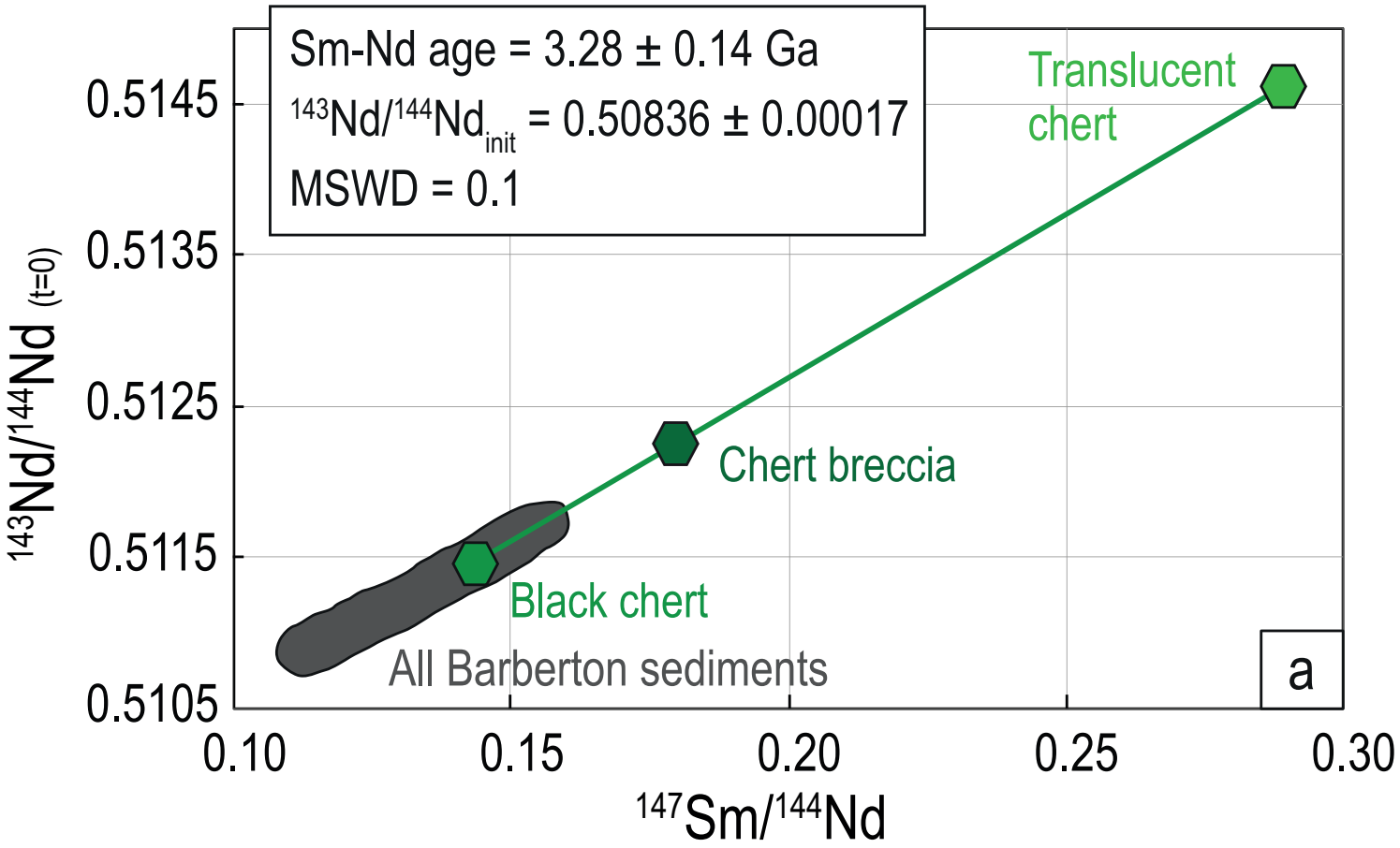

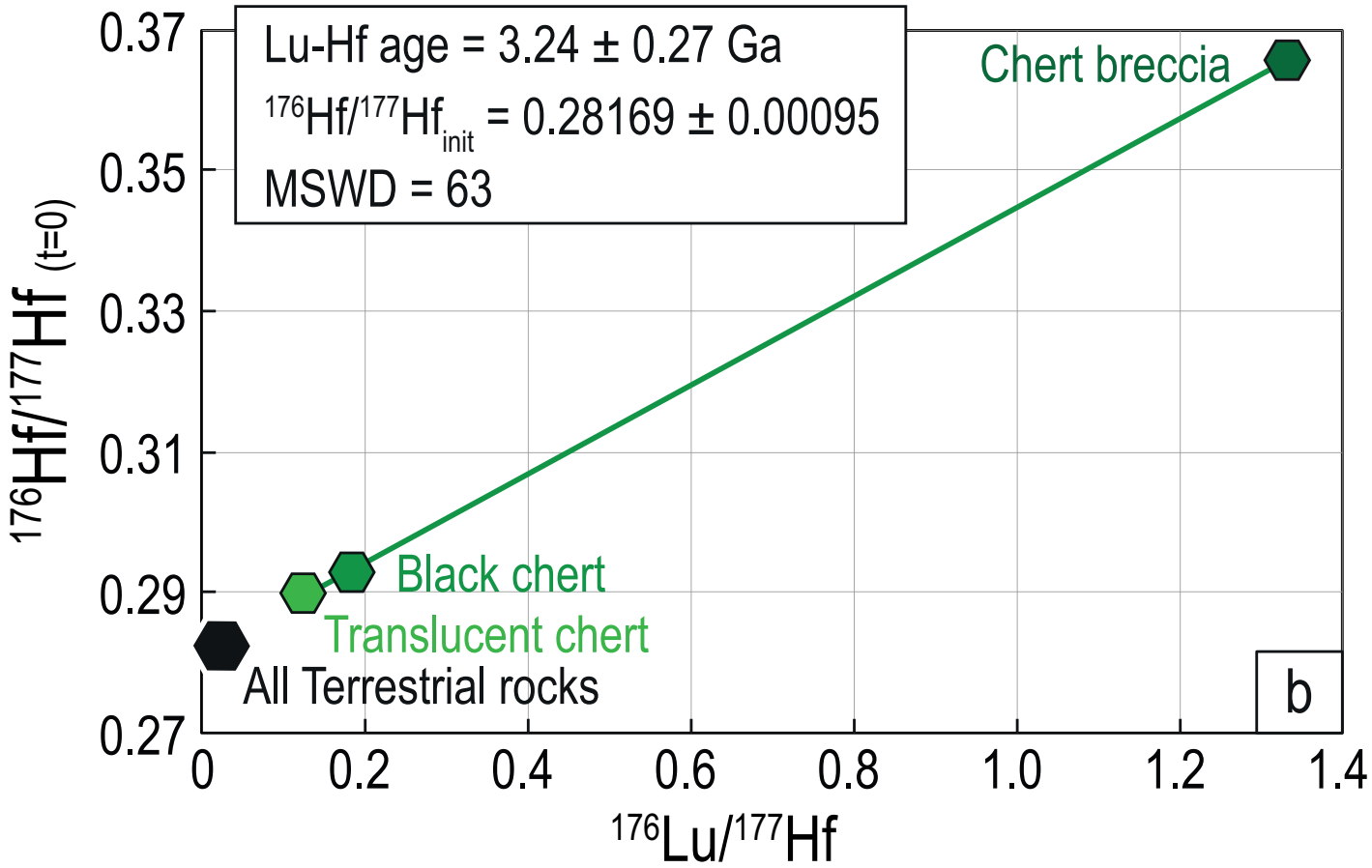

Figure 13

Figure 13

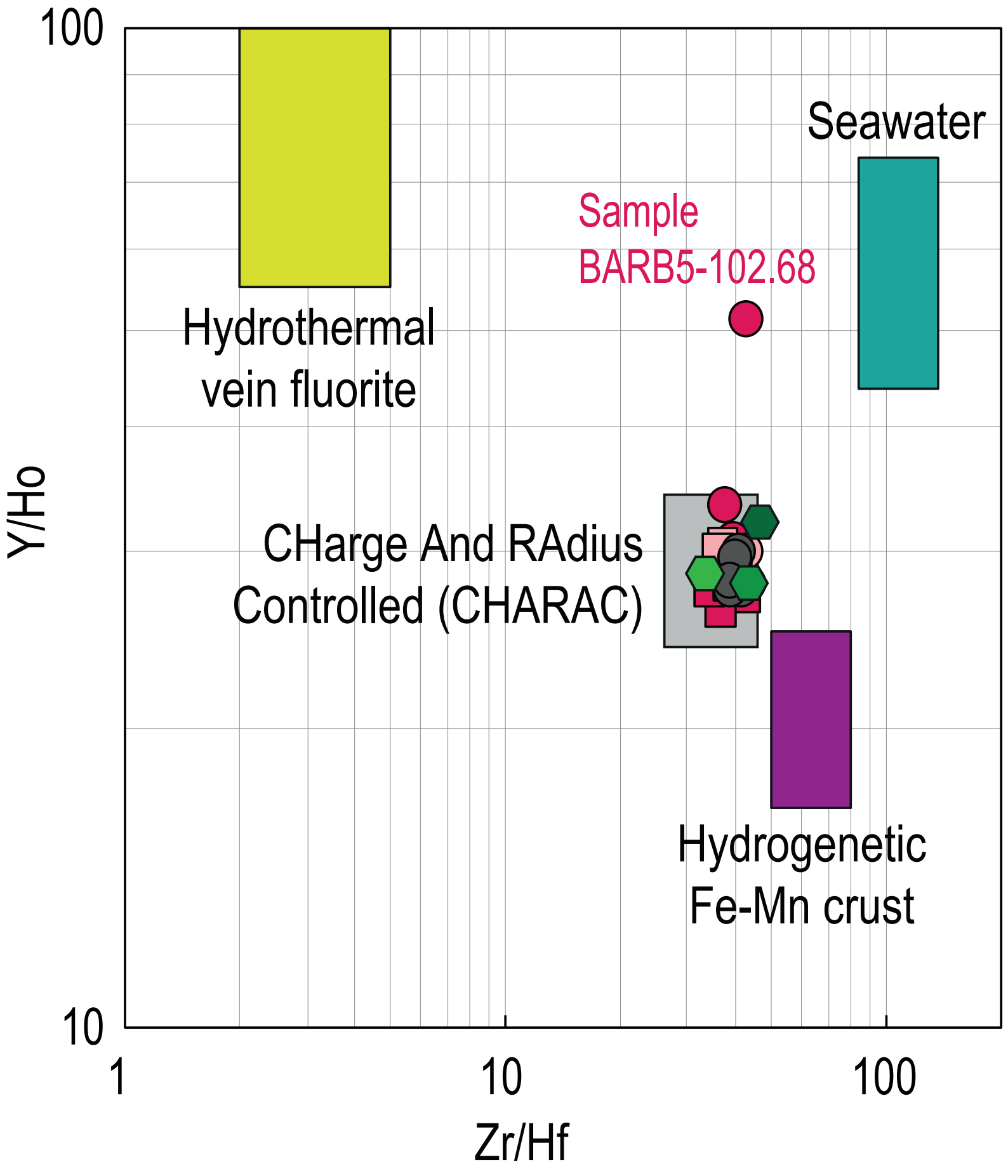

Supplementary Table A

Click here to download Electronic Annex: Supplementary Table A.xlsx

Supplementary Table B

Click here to download Electronic Annex: Supplementary Table B.xlsx

Supplementary File A

Click here to download Electronic Annex: Supplementary File A.pdf

Supplementary File B

Click here to download Electronic Annex: Supplementary File B.pdf

Supplementary File C

Click here to download Electronic Annex: Supplementary File C.pdf